



AALBORG UNIVERSITET
STUDENTERRAPPORT

In-silico modelling of cardiopulmonary interactions for estimating pulse pressure variation under conditions of respiratory muscle activity

Lasse Leuchtmann



28/02/2024



AALBORG UNIVERSITY
STUDENT REPORT

**Second year of masters degree at Department of Health
Science and Technology**

Biomedical Engineering and Informatics

Selma Lagerløfs Vej 249

9260, Gistrup

<https://www.hst.aau.dk>

Project topic:

Masters project: In-silico modelling of cardiopulmonary interactions for estimating pulse pressure variation under conditions of respiratory muscle activity

Project period:

September 2023 - february 2024

Participants:

Lasse Henrik Bech Leuchtmann

Supervisors:

Stephen Edward Reese

Pages report: 56

Pages appendix: 46

Pages total: 102

Finished: 1st of march, 2024

Abstract:

Introduction Patients receiving mechanical ventilation (MV) often require fluid resuscitation, due to e.g. sepsis or trauma. However, only 50% of patients are capable of adapting their cardiac output (CO) in response to fluid resuscitation. The ability to adapt is termed fluid responsiveness (FR). Pulse pressure variation (PPV) is a reliable biomarker for predicting FR. However, PPV is unreliable when respiratory muscle activity (P_{mus}) occurs. This study hypothesises a method for augmenting the PPV signal with an extra indice, -PPV, derived from the effect of pressure support (PS) variation on P_{mus} . The study conducted research into construction of a physiological model capable of predicting +PPV/-PPV. **Methods** A respiratory model based on the equation of motion (EOM), an intrathoracic model employing the α parameter and a cardiovascular model were combined with a feature extraction and optimization framework to predict +PPV/-PPV, and tested on data from a clinical trial researching the hypothesis. **Results** The model predicted +PPV/-PPV accurately on average, with all but one test resulting in $\Delta mean < 0.55\%$. Furthermore, the model predicted +PPV with $R^2 = 19$ and $R^2 = 0.62$, performing best at high PS timeframes. **Discussion** The models predictions were most accurate in conditions of positive intrathoracic pressure (P_{it}), and performance decreased at conditions of negative P_{it} . Thus, it is hypothesised that augmenting the models SB module as well as the data processing and extraction phases could improve the models g performance. Testing on a larger sample size is necessary to generalize this conclusion. **Conclusion** The cardiopulmonary model was capable of relatively accurately predicting the +PPV/-PPV signal at conditions of high P_{it} , and it is hypothesised that research into the SB module could improve performance on the entire signal.

Preface

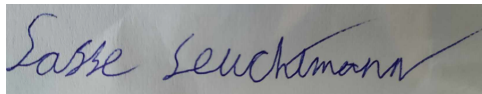
This study aimed to support research into the hypothesis that pulse pressure variation (PPV) can be augmented by changes in respiratory muscle activity P_{mus} due to PS variations, overcoming a common limitation of PPV. The study researched, designed and build a model of the cardiopulmonary interactions, capable of predicting PPV as well as -PPV, the extra indice derived from the hypothesis. The prediction of both indices simultaneously will consecutively be termed +PPV/-PPV. By combining a respiratory model based on the equation of motion (EOM), an intrathoracic model introducing the α parameter, and a cardiovascular model, as well as a parameter and input extraction and optimization framework, +PPV/-PPV was predicted. The predictions had a non-trivial accuracy, however limitations apply to the conclusion of the results.

This thesis was supervised by Professor Stephen Edward Rees in the period September the 3rd to the 29th of february 2024. A big thanks is given to Stephen Edward Rees for supervising this project!

Literature

In this project, when referring to literature, the Harvard method has been used. If a source only has one author, the author's surname followed by the published year of the source will be shown e.g. [Cryer, 1999]. If the source has multiple authors, the main author's surname is used followed by "et al." and the year the source was published e.g. [Vu et al., 2020].

If the source is used actively, the name of the author will be unbracketed and the year will be bracketed, eg. Seo et al. [2019]

A handwritten signature in blue ink that reads "Lasse Leuchtman". The signature is written in a cursive style with a long horizontal stroke at the end.

Lasse Henrik Bech Leuchtman

Contents

1	Introduction	1
2	Problem Analysis	3
2.1	Mechanical Ventilation	3
2.1.1	Purpose of Mechanical Ventilation	3
2.1.2	Associated Risks	3
2.1.3	Positive vs. Negative Pressure Ventilation	3
2.1.3.1	Mechanical and physiological differences	3
2.1.3.2	Historical Perspective	4
2.1.3.3	Pressure Waveform Differences	4
2.2	Equation of Motion	5
2.2.1	Derivation of the Equation of Motion	5
2.3	Esophageal Manometry	7
2.4	In-silico experimentation	8
2.4.1	Advantages and disadvantages of in-silico experiments	8
2.5	Cardiopulmonary Interactions	8
2.5.1	Affected anatomical compartments	8
2.5.2	Physiological Interactions	10
2.5.3	Clinical Significance of Cardiopulmonary Interactions	11
2.5.4	Fluid Responsiveness	11
2.5.5	Limitations of PPV as predictor of fluid responsiveness	11
2.6	Physiological Mechanisms Supporting the Project's Hypothesis	12

2.6.1	Effects of PS on P_{mus}	12
2.6.2	PPV Resulting from PS Changes	12
2.7	Hypothesis	13
3	Problem statement	14
4	Requirements Specification	15
5	Testing Framework Description	18
5.1	Cardiopulmonary interactions testing framework	18
5.1.1	Cardiopulmonary Interactions	18
5.1.2	Technical Solution to Problem Statement	19
5.1.2.1	Derive Model Parameters	19
5.1.2.2	Model PPV & Patient PPV	19
5.1.2.3	Compare Results	19
5.1.2.4	Hypothesis Conclusion	20
6	Methods	21
6.1	Respiratory Module	21
6.1.1	System of Equations	23
6.1.2	Driver Functions	23
6.1.3	Differential Equations for Simulating the Respiratory System	25
6.2	Intrathoracic Pressure Module	27
6.2.1	Equations	27
6.3	Cardiovascular Module	27

6.4	Simulation and Testing Framework	28
6.4.1	Respiratory Simulation Algorithm	28
6.4.1.1	Step 1 - Estimate R_{aw}	30
6.4.1.2	Step 2 - Estimate C_{rs}	30
6.4.1.3	Step 3 - Estimate P_{mus}	30
6.4.1.4	Step 4 - Extract Inspiratory & Expiratory time	31
6.4.1.5	Step 5 - Risetime and Deflation Time	32
6.4.1.6	Step 6 - Remaining Input Extraction and Breath Simulation	33
6.4.2	Pulse Pressure Variation Simulation Algorithm	33
6.4.2.1	Simulate Cardiovascular System	33
6.4.2.2	Simulate Cardiopulmonary Interactions	35
6.4.2.3	Step 6 - Extract +PPV/-PPV	36
6.4.3	Compare results	37
6.4.3.1	Coefficient of Determination	38
6.5	Parameter Optimization Framework	39
7	Results	41
7.1	System Requirement Testing	41
7.1.1	SR02 + SR03 + SR04	41
7.1.2	SR05	41
7.1.3	SR06	42
7.2	Individual Chunk Results	44
7.3	Full Patient Data	45

7.3.1 Patient 2	45
7.3.2 Patient 3	48
8 Discussion	52
9 Conclusion	56
10 Bibliography	57
A Validation Test Protocol for UR03	61
B Validation Test Protocol for UR04	62
C Validation Test Protocol for UR05	63
D Validation Test Protocol for SR01	64
E Validation Test Protocol for SR02 + SR03 + SR04	66
F Validation Test Protocol for SR05	67
G Validation Test Protocol for SR06	69
H Respiratory Module	71
I Anatomy of Mechanical Ventilation	73
J Transmural pressures	75
K Anatomy of the Pleural Cavity	76
L Historical Perspective of Esophageal Manometry	77

L.0.1	Complexity of Administering Esophageal Manometry	77
M	CircAdapt	78
M.1	Cardiovascular Module	78
M.1.1	Node Component Hierarchy	80
M.1.2	Patch Component Hierarchy	83
M.1.3	Connector component hierarchy	85
M.1.4	87
M.1.5	Wall Component Hierarchy	87
N	Model Performance on Individual Timechunks	88
N.0.1	Blood Pressure Predictions	93
N.0.2	Timeframe 1 - PS 18.1	93
N.0.3	Timeframe 2 - PS 13.1	97
N.0.4	Performance on entirety of patient data	101

1 | Introduction

Respiratory failure defines the body's inability to adequately perform external respiration. Treatment of respiratory failure often requires the patient to be put on mechanical ventilation (MV). [Yoder, 2016]

In 2021, 27,487 patients were admitted to the ICU in Denmark. Of these, 13,096, corresponding to 47.6%, received mechanical ventilation. [Dansk Intensiv Database, 2021] Furthermore, a total of 1,596 patients were admitted to the ICU for COVID-19 treatment. Out of these, 898, corresponding to 56.14%, received mechanical ventilation. [Dansk Intensiv Database, 2021]

Patients under MV often suffer conditions which require fluid resuscitation, e.g. sepsis or trauma. Sepsis reduces induces hypovolemia, decreases tissue perfusion and as a result O_2 delivery. Trauma can lead to acute blood loss, activating hemodynamic responses to restore volume. [Wallace and Regunath]

The purpose of fluid resuscitation is to increase cardiac output (CO) and organ perfusion, in order to restore hemodynamic stability [Wallace and Regunath]. 60% of patients which develop ARDS receive inotropics, with the majority being administered fluid resuscitation [Carvalho et al.].

The ability of a patient to adapt CO to the increase in blood volume, is termed fluid responsiveness (FR). However, only 50 % of patient administered fluid resuscitation, are FR. [Tre Boul et al., 2018]

Several biomarkers exist to predict FR. The most reliable of these, is pulse pressure variation (PPV). [Tre Boul et al., 2018]

PPV is a measure of the changes in arterial pressure during the respiratory cycle, often measured at the pulmonary artery (P_{pa}). PPV occurs as a result of cardiopulmonary interactions, wherein changes in plural pressure (P_{pl}) during respiration, affect intrathoracic pressure (P_{it}). The change in P_{it} is then transduced to P_{pa} changes, resulting in variation of the pulse pressure.

However, PPV is unreliable when spontaneous breathing (SB) or cardiac arrhythmias occur. Thus, research into novel methods for FR prediction capable of overcoming these limitations are necessary. [Tre Boul et al., 2018]

This study aimed to investigate a hypothesis, which proposes a novel method for overcoming the limitations imposed on PPV as a predictor of FR.

The foundation of the hypothesis, is based on interactions that pressure support (PS) MV has on respiratory muscle activity. Increasing PS reduces respiratory muscle activity. Conversely, reducing PS increases

respiratory muscle activity. [Roesthuis et al.; E. Brackett and Sanghavi; Duiverman et al.]

Thus, by applying physiological knowledge and advanced signal processing, it is hypothesised that PS is able to augment the PPV signal in a way that overcomes its limitations.

This study aims to investigate the hypothesis via in-silico experimentation, using statistical comparison with data obtained from in-vivo clinical experimentation to conclude on the hypothesis' feasibility.

2 | Problem Analysis

2.1 Mechanical Ventilation

Understanding the issues associated with the project's hypothesis, necessitates knowledge of mechanical ventilation.

2.1.1 Purpose of Mechanical Ventilation

Mechanical ventilation (MV) is a supportive intervention used to sustain respiratory function in patients with acute respiratory failure. MV strives to provide the patient with proper oxygenation, eliminate CO_2 , and to support the patients work of breathing (WOB) [Zhang et al., 2019].

See appendix I for the anatomy of a mechanical ventilator.

2.1.2 Associated Risks

Though MV is a necessity in treating patients with critical respiratory condition, patients receiving MV treatment also risk developing ventilator associated events (VAE) as a result of the treatment. VAE's can worsen the patient's health status, increase length of stay and even increase patient morbidity.[Ochiai, 2015] Thus, it is essential to wean patients from the ventilator as quickly and efficiently as possible.

Weaning a patient can be a difficult process. While weaning a patient in pressure support (PS) mode, a balance should be struck between supporting the patient enough to reduce excessive work of breathing (WOB), and preventing atrophy of the respiratory muscles [Reese et al., 2018]

2.1.3 Positive vs. Negative Pressure Ventilation

Different modalities of mechanical ventilation are capable of performing external respiration. Understanding the underlying physiology of these modalities, provides a basis for understanding the cardiopulmonary interactions.

2.1.3.1 Mechanical and physiological differences

Mechanical ventilation devices can be divided into two main modalities. These modalities are positive pressure ventilation (PPVENT) and negative pressure ventilation (NPVENT). The main differences between these categories of MV, are described in table 2.1

As described in table 2.1, the effects of NPVENT are identical with those of spontaneous breathing (SB),

PPVENT	NPVENT
Inflation of the lungs occurs due to pressure created by the ventilator	A compartment enclosing the chest wall creates a negative transthoracic pressure, inflating the lungs
P_{pl} is positive during inspiration	P_{pl} is negative during inspiration
Only possible during MV	Occurs in NPVENT MV treatment, as well as during spontaneous breathing

Table 2.1: The main differences between PPVENT and NPVENT

though the effects are achieved through different mechanisms.

2.1.3.2 Historical Perspective

Historically, experimental devices with functions similar to PPVENT were invented before NPVENT, in the 16th century [Pham et al., 2017]. However, in modern medicine, NPVENT was applied as treatment for polio at the end of the 19th century, with continued usage until the mid 20th century. During the 1950's however, PPVENT was introduced into clinical practice, and currently remains the main technique for administering MV. [Pham et al., 2017]

2.1.3.3 Pressure Waveform Differences

Due to the differences in how PPVENT and NPVENT impact the patient's respiratory physiology, the corresponding P_{ao} waveforms will differ. These differences are illustrated in figure 2.1

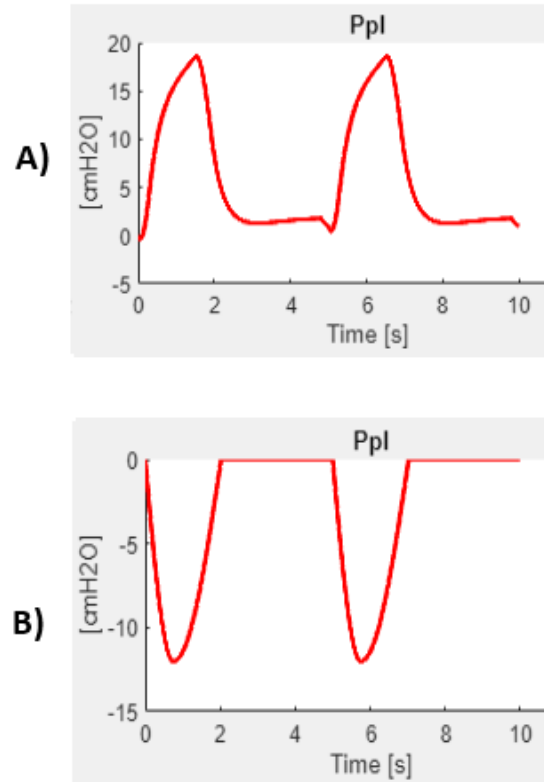


Figure 2.1: Waveform differences between PPVENT and NPVENT. A) depicts the positive pressure delivered by the ventilator. B) depicts the negative pressure caused by either contraction of the respiratory muscles during SB, or a NPVENT device. Baseline pressure for both waveforms is PEEP.

Fig 2.1 depicts, how the pressure waveform stays positive throughout PPVENT, and negative throughout NPVENT, with respect to PEEP as baseline pressure.

2.2 Equation of Motion

The equation of motion (EOM) is a well-established mathematical model within the respiratory research community, for simulating various aspects of the respiratory system. [Vicario et al., 2015]

2.2.1 Derivation of the Equation of Motion

The EOM is derived from a compartment model of the lungs, termed the linear first-order single-compartment model of respiratory mechanics (LFOSCM). [Vicario et al., 2015; Albanese et al., 2013] The LFOSCM is depicted in figure 2.2.

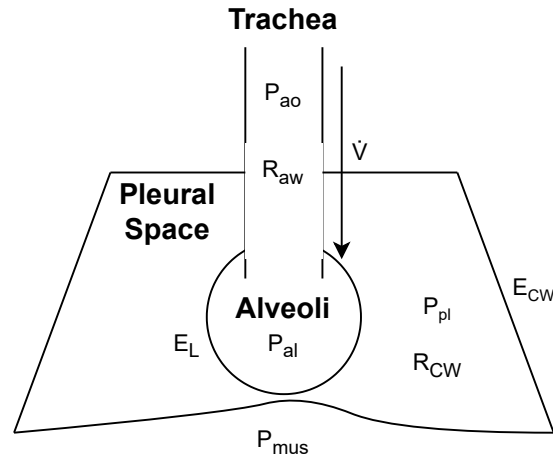


Figure 2.2: Visualization of the LFOSCM. Depicted are the trachea, pleural space and the alveoli. Variables P_{ao} , P_{al} , P_{pl} & P_{mus} denote pressure at the airway opening, at the alveoli, in the pleural space and pressure exerted by the respiratory muscles, respectively. Parameters R_{aw} & R_{CW} denote airway- and chestwall resistance, respectively. E_L & E_{CW} denote elastance of the lungs- and chestwall, respectively. \dot{V} denotes the airflow across the respiratory system. Adapted from Vicario et al. [2015].

The bioelectrical analogue of the LFOSCM is depicted in figure 2.3a. In figure 2.3a, \dot{V} denotes the airflow across the system. The pressure delivered by the mechanical ventilator is P_{ao} . The pressure drop across R_{aw} creates a differential pressure at the alveoli, P_{al} . Lung elastance E_L is analogous to a capacitance. Friction within the chest wall is accounted for by R_{cw} , and the elastance of the chest wall is denoted by E_{cw} . P_{mus} is the pressure exerted by the respiratory muscles. Vicario et al. [2015]

Figure 2.3b describes the LFOSCM, but but as a lumped parameter model. In the lumped model, R_{aw} and R_{CW} are lumped together in a single resistance parameter, R . Similarly, E_L and E_{CW} are lumped together as E . Lastly, the pressure sources have been reduced to P_{ao} and P_{mus} [Bates H. T., 2009].

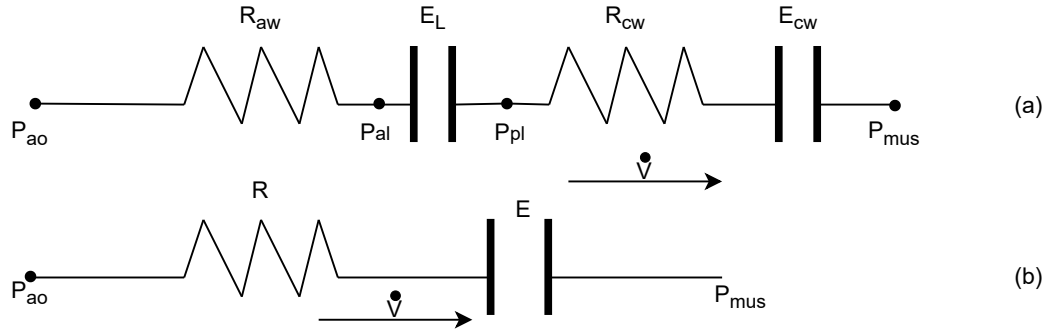


Figure 2.3: The bioelectrical analogue of the LFOSCM. In a), \dot{V} is the airflow across the system. P_{vent} is supplied by the ventilator. R_{aw} creates a pressure gradient, resulting in P_{al} . E_L is analogous to a capacitance. R_{cw} and E_{cw} are friction and elastance within the chest wall, respectively. P_{mus} is the pressure supplied by the respiratory muscles. b) describes bioelectrical analogue as a lumped parameter model, from which the EOM is derived.

From figure 2.3b, the EOM can be derived. Eq 2.1 describes the EOM.

$$P_{vent}(t) = R\dot{V}(t) + EV(t) + P_{mus}(t) + PEEP \quad (2.1)$$

2.3 Esophageal Manometry

Due to the anatomy of the pleura detailed in appendix K, P_{pl} measurements cannot be directly recorded. In clinical practice, P_{pl} is thus estimated through esophageal manometry (EM), which is not a routine measurement.

EM is performed by placing an esophageal catheter with a pressure transducer attached to a balloon in the patients esophagus. This procedure measures esophageal pressure (P_{eso}), which is used as a surrogate for P_{pl} [Grieco L. and Chen L, 2017] The esophageal pressure measurements are then validated one of two ways. Either through a negative pressure occlusion test, by thorax compression during end-expiratory pause, or a Baydur test, by occluding the airways during inspiration [Chiumello et al., 2016]. If the balloon is either inflated too much or too little during measurement, the values may not correctly reflect the esophageal pressure. [Grieco L. and Chen L, 2017] Thus, esophageal manometry is a complicated procedure with a risk of collecting distorted data.

Refer to appendix L for the historical perspective on EM, as well as a breakdown of different modalities.

Even though esophageal manometry is the clinical standard for measuring P_{eso} , in-silico modelling exists

to estimate P_{eso} non-invasively.

2.4 In-silico experimentation

In-silico experimentation, is a way to perform scientific experiments via computational modelling. [Barh et al., 2013] Silico refers to silicum, which is a foundational building block of MOSFETs, enabling construction of logic gates within most CPU's.

The origin of the term in-silico modelling is unknown. However, according to Barh et al. [2013], some of the earliest uses of the term can be traced to Sieburg [1990] and Danchin et al. [1991].

2.4.1 Advantages and disadvantages of in-silico experiments

in-silico experimentation provides opportunities within scientific experimentation, which are often limited in in-vivo or in-vitro experiments [Barh et al., 2013]. Table 2.2 outlines some of the major advantages as well as disadvantages of in-silico experimentation.

Advantages	Disadvantages
Reduced need for trial subjects	Difficulty in accounting for all factors influencing a phenomena
Reduced resource allocation for experiments	in-silico experimentation must be validated by in-vivo or -vitro experiments to support the conclusion
Enables experiments which would otherwise be impossible due to ethical reasons, lack of resources or lack of essential expert knowledge	

Table 2.2: Some of the major advantages and disadvantages of in-silico experimentation

2.5 Cardiopulmonary Interactions

Cardiopulmonary interactions occur as a result of intrathoracic pressure changes during the respiratory cycle, which affect the cardiovascular system in various ways.

2.5.1 Affected anatomical compartments

As seen in figure 2.4, several compartments and their encapsulated organs are affected by the cardiopulmonary interactions.

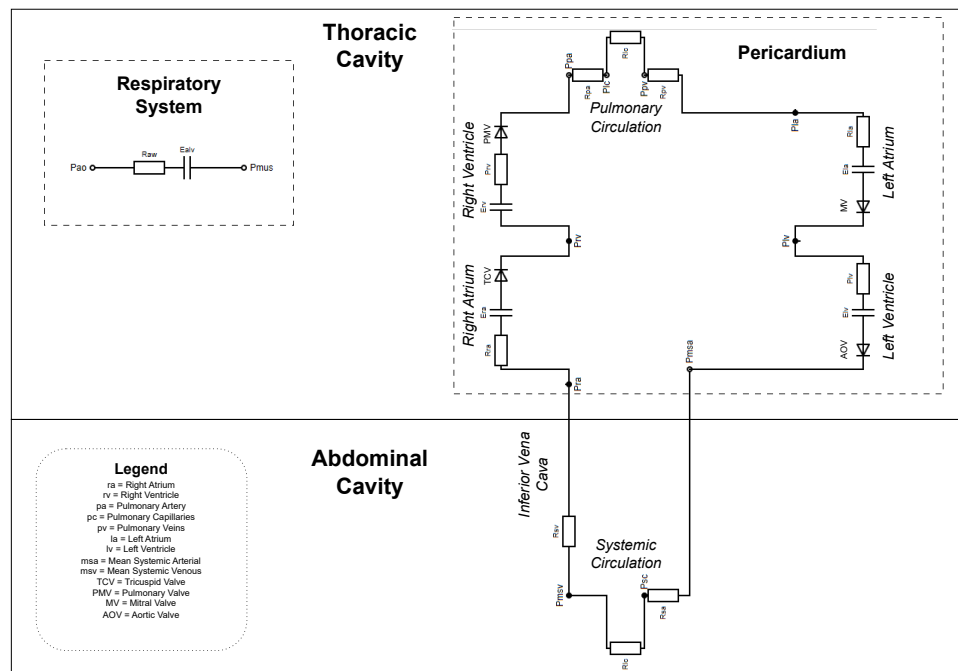


Figure 2.4: Bioelectrical modelling of the compartments and organs of interest affected by the cardiopulmonary interactions. The EOM models the respiratory system, and the corresponding ΔP_{pl} during the respiratory cycle, affects the intrathoracic cavity and abdominal cavity. The pericardium, which encapsulates the heart, resides within the intrathoracic cavity. The inferior vena cava resides within the abdominal cavity.

table 2.3 shows which compartments and organs within the thoracic and abdominal cavities are affected by the cardiopulmonary interactions.

Affected Compartment	Affected Organs
Thoracic Cavity	
Pleural Cavity	<i>Lungs</i>
Pericardium	<i>Heart, pulmonary circulation</i>
Abdominal Cavity	
Systemic Circulation	<i>Inferior Vena cava</i>

Table 2.3: The compartments and organs affected by cardiopulmonary interactions within the thoracic and abdominal cavities.

Thus, as depicted in figure 2.4, within the thoracic cavity, the respiratory system, the heart and the pulmonary circulation are affected by ΔP_{pl} during the respiratory cycle. In the abdominal cavity, the inferior vena cava is the main organ of interest affected by ΔP_{pl} .

2.5.2 Physiological Interactions

In the following subsection, the effects which will be described are based on an increase in P_{pl} , such as that occurring during inspiration at PPVENT, or expiration at NPVENT. The effects will be reversed in accordance with negative intrathoracic pressure (P_{it}).

As seen in figure 2.1A, cyclical P_{pl} variations occur during the respiratory cycle.

These changes in P_{pl} are transduced to P_{it} by a factor α [Cushway et al., 2022].

Bloodflow through the cardiovascular system can be described via ohms law, exchanging voltage for pressure, as described in eq. (2.2). [Feher, 2017]

$$flow = \frac{P1 - P2}{R} \quad (2.2)$$

Right Heart Effects

When P_{it} increases, transmural pressure across the right atrium (RA) decreases. In accordance with eq. (2.2), the resulting effect is reduced bloodflow. This in turn reduces RA and right ventricle (RV) preload. Reduced RV preload, reduces pulmonary artery pressure (P_{pa}). Finally, RV afterload increases. [Pinsky, 2017]

Left Heart Effects

Reduced RV preload reduces LV preload. This in turn decreases stroke volume (SV). The increased P_{it} is said to serve as a left ventricular assist device, being that it decreases LV afterload. [Pinsky, 2017]

Table 2.4 provides a quick overview of the effects of the cardiopulmonary interactions. These effects are from the perspective of increased P_{pl} .

Right Heart	Left Heart
Systemic Venous Return ↓	N/A
Afterload ↑	Afterload ↓
Preload ↓	Preload ↓

Table 2.4: An overview of the main effects of the cardiopulmonary interactions. The effects are from the perspective of an increase in P_{pl} , and are reversed when P_{pl} decreases.

2.5.3 Clinical Significance of Cardiopulmonary Interactions

The described cardiopulmonary interactions, enact several phenomena of clinical significance. Of these phenomena, pulse pressure variation (PPV) is of interest for this project, since it adds a second signal to the P_{pa} measurements, which directly correlates with ΔP_{it} occurring from ΔP_{pl}

PPV is a measure of the change in arterial pulse pressure, as a consequence of ΔP_{it} during the respiratory cycle. [Trebloul et al., 2018]

In a patient undergoing PPVENT, ΔP_{it} will be positive during inspiration, and cycle towards baseline during expiration. Thus, P_{pa} will be higher during inspiration, and lower during expiration. [Trebloul et al., 2018]

Since PPV depends on ΔP_{it} as a consequence of the respiratory cycle, it essentially augments P_{pa} with a secondary signal, which is independent of the cardiac cycle.

2.5.4 Fluid Responsiveness

In MV patients, PPV is a valid predictor of fluid responsiveness (FR). FR is defined, as the ability of the patients LV to increase SV by 10-15% in response to administration of 500mL crystalloid fluid. [Trebloul et al., 2018]

The underlying hypothesis for PPV as a biomarker for FR, is that large respiratory changes to LV SV, occur when the patient is biventricular. Trebloul et al. [2018]

Eq eq. (2.3) shows how likely the patient is to be fluid responsive, based on their PPV. [Trebloul et al., 2018]

$$\text{Fluid responsiveness} = \begin{cases} \text{High likelihood} & \text{if } PPV > 13\% \\ \text{Gray Area} & \text{if } 9\% < PPV < 13\% \\ \text{Unlikely} & PPV < 9\% \end{cases} \quad (2.3)$$

2.5.5 Limitations of PPV as predictor of fluid responsiveness

When relying on PPV for predicting a MV patient's FR, the limitations of its use must be understood. Thus, if cardiac arrhythmias or spontaneous breathing occur, PPV should not be considered a predictor of FR. [Trebloul et al., 2018]

Due to these limitations, research should be conducted on methods to make PPV applicable in conditions

where the limitations are present. Treboul et al. [2018]

2.6 Physiological Mechanisms Supporting the Project's Hypothesis

This project proposes a novel method for augmenting the PPV signal, in such a way that it is applicable in conditions where its limitations otherwise negate its validity.

To understand the hypothesis, insight into two physiological mechanisms is required:

2.6.1 Effects of PS on P_{mus}

The first physiological mechanism, relates to the way PS interacts with P_{mus} .

In patients undergoing MV, the level of PS impacts the patient's respiratory muscle activity. Studies show that increased PS counteracts respiratory muscle activation, thus reducing P_{mus} , whereas the inverse relationship holds for decreased PS. [Roesthuis et al.; E. Brackett and Sanghavi; Duiverman et al.]

Assuming validity of this relationship, P_{mus} can be assumed to be 0 at high levels of PS. Thus, under these conditions, C_{rs} can be calculated as described in eq. (2.4).

$$C_{rs} = \frac{\Delta V}{\Delta P} \quad (2.4)$$

If C_{rs} is known, P_{mus} can thus be estimated at varying levels of PS, as described in eq. (2.5).

$$P_{mus} = \left(\frac{V_t - (PS * C_{rs})}{C_{rs}} \right) \quad (2.5)$$

Eq 2.5 subtracts the V generated by PS from V_t . Thus, the remainder of V must be a result of P_{mus} .

2.6.2 PPV Resulting from PS Changes

As a result of the mechanism described in section 2.6.1, PPV variations occur due to differing PS levels.

Sec 2.5 describes the underlying physiology of the cardiopulmonary interactions. Thus, when PS is high, P_{pl} is assumed to be maximal at inspiration and minimal at expiration. Conversely, when PS is low, P_{pl} is assumed to be minimal at inspiration, and maximal at expiration.

Following this assumption, $P_{insp}Max - P_{exp}min$ (+PPV) provides an indice for the effect of PS on PPV. Similarly, $P_{Exp}Max - P_{insp}Min$ (-PPV) provides an indice for the effect of P_{mus} on PPV.

Thus, if P_{mus} , as well as both +PPV/-PPV are known at every respiratory cycle, the PPV signal is effectively augmented by the changes in PS.

2.7 Hypothesis

The physiological mechanisms described in section 2.6.1 and section 2.6.2, provide basis for the following hypothesis:

"PPV can be used to estimate FR during conditions where SB occurs, by combining +PPV/-PPV at the highest and lowest PS settings"

3 | Problem statement

The hypothesis described in 2.7 requires experimental evidence in order to be confirmed. Due to the advantages of in-silico experimentation outlined in section 2.4, performing the experiment in a simulated environment would significantly reduce its associated resource costs. Thus, invention of a computational model capable of predicting +PPV/-PPV is a necessity for creating the experiment in-silico.

The problem statement of this project is:

"How can a physiological model be designed and implemented, to predict +PPV/-PPV in pressure support mechanically ventilated patients?"

4 | Requirements Specification

From the problem analysis conducted in chapter 2, a set of user- and system-requirements for the technical solution to the problem statement were derived.

The requirement specification is accompanied by a set of test protocols, which can be found in appendix A to appendix G.

Requirement ID	Requirements
UR_1	The solution must function with routinely available patient data
UR_2	The solution must be operational out-of-box and require minimal adaptation from the user
UR_3	The solution must be able to simulate pressure support mechanical ventilation administered in the clinical trials
UR_4	The solution must be able to simulate cardiopulmonary interactions based on the clinical trial data
UR_5	The solution must be able to simulate the surrogate P_{mus} derived from the clinical trials
UR_6	The solution must be able to perform statistical comparisons between the surrogate P_{mus} and the simulated P_{mus}

Table 4.1: User requirements for the solution to the problem statement

Requirement ID	Requirements
SR_1	The system must be able to simulate the patient's respiratory physiology
SR_1_1	State variables and parameters constituting the respiratory physiology must include, but not be limited to: <ol style="list-style-type: none"> 1. V_t 2. P_{aw} 3. C_{rs} 4. flow 5. R_{aw}
SR_2	The system must be able to simulate the intrathoracic pressure changes occurring as a result of respiration
SR_2_1	State variables constituting intrathoracic changes must include, but not be limited to: <ol style="list-style-type: none"> 1. P_{it}
SR_3	The system must be able to simulate the cardiovascular system
SR_3_1	State variables & inputs constituting the cardiovascular system must include, but not be limited to: <ol style="list-style-type: none"> 1. P_{pa} 2. \dot{V}_{pa} 3. V_{pa} 4. C_{pa} 5. P_{ra} 6. \dot{V}_{ra} 7. V_{ra} 8. C_{ra} 9. P_{rv} 10. \dot{V}_{rv} 11. V_{rv} 12. C_{rv}
SR_4	The system must be able to simulate the cardiopulmonary interactions
SR_5	The system must be able to simulate spontaneous breathing
SR_5_1	The system must be able to simulate respiratory muscle activation -

Table 4.2: System requirements for the system which can fulfill the user requirements.

Requirement ID	Requirements
SR_5_1_1	<p>State variables & inputs constituting respiratory muscle activation must include, but not be limited to:</p> <ul style="list-style-type: none"> • P_{mus} • C_{rw}
SR_6	The system must be able to simulate positive pressure ventilation
SR_6	<p>State variables constituting positive pressure ventilation must include, but not be limited to:</p> <ul style="list-style-type: none"> • T_{insp} • TCT • T_{rise} • PS • $PEEP$ • <i>Cycle Variable</i> • <i>Respiratory Rate</i> • τ

Table 4.3: System requirements for the system which can fulfill the user requirements (Continued)

5 | Testing Framework Description

5.1 Cardiopulmonary interactions testing framework

Based on the requirements derived in chapter 4, a framework for testing the hypothesis described in chapter 3 was derived. The framework consists of a mathematical model of the cardiopulmonary interactions, combined with a testing and validation framework, which together allow for validation of the hypothesis. The architecture of this framework is presented in figure 5.1.

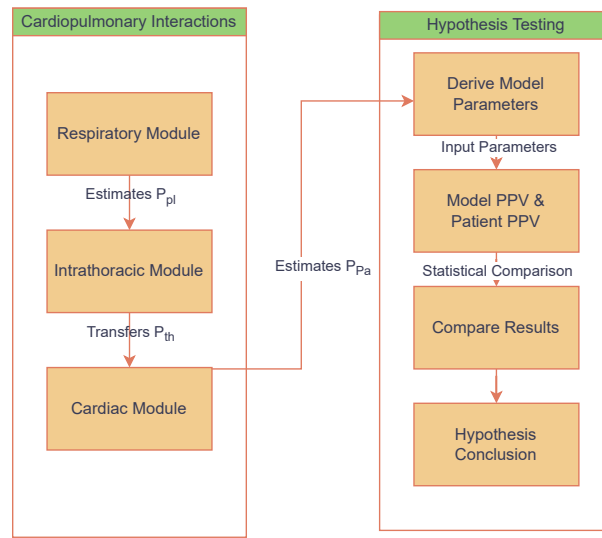


Figure 5.1: Architecture of the integrated mathematical model and hypothesis testing framework

5.1.1 Cardiopulmonary Interactions

Based on the cardiopulmonary interactions described in section 2.5, a mathematical model will be built, which simulates their underlying physiology. This model consists of three modules, each simulating a section of the cardiopulmonary interactions.

Respiratory Module

The respiratory module, aims to simulate the respiratory physiology of a patient undergoing PS MV. The mathematical modelling of the respiratory physiology, will be derived from the EOM.

The ventilator model will be implemented as an extension module, integrated within the respiratory module. Thus, the model will be able to simulate various aspects of the ventilator, such as rise time,

cycle variables, PEEP etc.

The respiratory model will also be able to simulate the activation of the patient's respiratory muscles during spontaneous breathing activity.

Intrathoracic Pressure Module

The intrathoracic pressure module, will act as an intermediary module between the respiratory- and cardiovascular module. Thus, it simulates the effect that changes in P_{pl} have on P_{it} , thus enabling transducing of P_{pl} to transmural pressure in the cardiovascular system.

Cardiovascular Module

The cardiovascular module will model the patient's cardiovascular system during MV, allowing for PPV estimation. Thus, the main purpose of the cardiovascular module is to mathematically simulate arterial pressure, which will be integrated with the intrathoracic pressure module in order to simulate the patient's PPV.

5.1.2 Technical Solution to Problem Statement

In order to test and conclude on the problem statement of chapter 3, a framework will be built to facilitate such testing. The framework will consist of several modules and processes, each facilitating a function necessary to derive a conclusion.

5.1.2.1 Derive Model Parameters

In the first process of the hypothesis testing framework, values of parameters necessary for model simulation will be extracted from the patient's data. For a full list of parameters and their method of derivation, please refer to section 6.1.

5.1.2.2 Model PPV & Patient PPV

In this process, the patients PPV will be extracted from the data, and simultaneously the mathematical model will simulate PPV based on the extracted parameters. Thus, the hypothesis can be tested by comparing the extracted and simulated PPV values.

5.1.2.3 Compare Results

In this process, the simulated and extracted PPV values will be compared via a coefficient of determination, as well as Bland-Altman plotting. Thus, it will be possible to conclude on the hypothesis.

5.1.2.4 Hypothesis Conclusion

Once the simulated and extracted PPV values are compared, it will be possible to draw a conclusion on whether or not it is possible to base P_{mus} estimations on C_{rs} at high PS levels. This conclusion will be made with respect to the assumptions and restrictions of the model.

6 | Methods

6.1 Respiratory Module

The purpose of the respiratory module, is to simulate the patient's breathing mechanics during respiration. The module simulates the respirators interaction with the respiratory system, as well as the patient's own spontaneous breathing. The patient's respiratory physiology is thus modelled as a system of governing equations, as well as a set of parameters necessary for simulating various respiratory properties.

The respiratory module's parameters and their method of derivation are shown in table 6.1

Parameters	Definition	Derivation Method
Mechanical Properties		
C_{rs}	Respiratory system compliance [$\frac{L}{cmH_2O}$]	$\frac{\Delta V}{\Delta P}$ at $P_{mus} = 0$
C_{cw}	Chest wall compliance [$\frac{L}{cmH_2O}$]	4% of vital capacity
Bulk Properties		
R_{aw}	Arway Resistance [$\frac{cmH_2O}{\frac{L}{s}}$]	Least-Square fitting on five breaths at $P_{mus}=0$

Table 6.1: Parameters of the respiratory module of the cardiopulmonary model

The respiratory module also takes a number of inputs, which simulate MV settings, characteristics of the respiratory muscle activation, as well as global simulation parameters.

These inputs are shown in table 6.2

Inputs	Definition	Derivation
Vent Settings		
PS	Pressure Support [cmH_2O]	PS of timeframe which clinical trial is performed at
PEEP	Positive end expiratory pressure [cmH_2O]	PEEP setting at timeframe
PSTrigger	Threshold for ΔP_{pl} needed for activating PS [cmH_2O]	Manually adjusted
TCT	Total cycle time \rightarrow Duration of respiratory cycle [s]	$t_{insp} + t_{exp}$
t_{insp}	Inspiratory time [s]	Positive flow time in patient data
t_{exp}	Expiratory time [s]	Negative flow time in patient data
Rise Time	Time from PSTrigger activating till PS level has been reached [s]	20% of t_{insp} (Manually adjustable)
RR	Respiratory rate [breaths/minute]	Manually set during model testing
P_{mus} Settings		
Ti P_{mus}	Inspiratory time for respiratory muscles [s]	Same as t_{insp}
Te P_{mus}	Expiratory time for respiratory muscles [s]	Same as t_{exp}
P_{mus} Set	Max P_{mus} [cmH_2O]	Surrogate P_{mus} calculated from clinical trial data
P_{mus} Deflation time	Time from end-inspiratory P_{mus} , until relaxed diaphragm	Manually set
P_{mus} Cycle	Threshold for P_{mus} cycling off [L/min]	Manually set
Simulation Parameters		
Δt	timestep at which model is simulated [s]	Synchronized with cardiovascular module
Simulation length	Total length of simulation [s]	manually set during model testing
Expiratory time constant	Time for respiratory system to empty 63% [s]	Manually set

Table 6.2: Table of the inputs needed to simulate patient breathing cycle

During the model's simulation of the patient's respiratory mechanics, a number of state variables are logged. The state variables are shown in table 6.3

State Variable	Definition	Derivation Method
P_{ao}	Pressure at airway opening [cmH ₂ O]	$\frac{\Delta V}{C_{rs}}$
\dot{V}	flow [L/min]	$\frac{P_{ao}-P_{pl}}{R_{aw}}$
V	Volume [L]	$\dot{v} * \Delta t$
P_{pl}	Pleural pressure [cmH ₂ O]	$\frac{V}{C_{cw}} + P_{mus} + P_{ao}$

Table 6.3: State variables of the respiratory module of the cardiopulmonary model

6.1.1 System of Equations

The underlying mechanics of the respiratory module, consist of a system of governing equations, derived from the EOM described in section section 2.2

The system is governed by two time-dependent driver functions, as well as a set of differential equations.

6.1.2 Driver Functions

Simulation of the ventilator's effect on the patient's respiratory physiology, as well as respiratory muscle activity, are implemented through the use of driver functions.

The driver functions each have time varying pressure profiles, which are build based on assumptions derived from knowledge of human respiratory physiology, as well as knowledge of the inner workings of MV.

Pvent driver profile

The profile of the inspiratory driver function has two states.

The states relate to whether drop in P_{pl} has reached the threshold set in the PSTrigger input variable.

eq. (6.1) describes the time dependent relationship of P_{vent} if PSTrigger has not been reached.

$$P_{vent}(t) = PEEP \mid \text{if } P_{pl} > PSTrigger \quad (6.1)$$

Thus, if P_{pl} has not dropped below the PSTrigger threshold, the pressure delivered by the ventilator will equal PEEP.

Eq 6.2 describes the time dependent relationship of P_{vent} , if the PSTrigger threshold has been reached during the respiratory cycle.

$$P_{vent} = \begin{cases} PS * \frac{t}{t_{rise}} + PEEP & \text{if } 0 < t \leq t_{rise}(1) \\ PS + PEEP & \text{if } t_{rise} < t \leq t_{insp}(2) \\ PS - (PS * (\frac{t}{t_{deflate}} + PEEP)) & \text{if } t_{insp} < t \leq t_{insp} + t_{deflate}(3) \\ PEEP & \text{if } t_{insp} + t_{deflate} \leq TCT(4) \end{cases} \quad (6.2)$$

Eq 6.2 consists of 4 phases.

1. When PSTrigger is activated, the vent starts delivering pressure. This pressure rises from PEEP to PS over the course of t_{rise} [Hess R., 2014].
2. When P_{vent} reaches PS, it remains there for the remainder of inspiration.
3. At the end of inspiration, pressure delivery decreases, reaching PEEP after $t_{deflate}$ has passed.
4. Until start of next inspiration, PEEP remains 0.

Pmus driver profile

The profile of the P_{mus} driver function simulates the pressure exerted by the patient's respiratory muscles. For a patient undergoing MV, P_{mus} is mainly exerted by contraction of the diaphragm, but if forced breathing occurs, the external- and internal intercostals would aid in P_{mus} generation.

The P_{mus} profile is infused with physiological knowledge regarding the nature of P_{mus} generation, which constitutes that P_{mus} rises monotonously during inspiration, decrements monotonously during expiration, and remains 0 between expiration and inspiration [Vicario et al., 2015].

Due to the monotonic and cyclical nature of SB at rest, the P_{mus} profile is implemented as a sine wave, with varying periods and phase shifts.

The P_{mus} profile has two states. The first state simulates a full inspiratory and expiratory cycle. The second state ends the inspiratory phase and begins expiration, once the flow threshold for the P_{mus} cycle variable is reached. The two states enable simulation of a full spontaneous breathing (SB) cycle, as well as prematurely ending the cycle if P_{mus} cycle variable is reached due to flow caused by increase in P_{vent} .

$$P_{mus} = \begin{cases} P_{musSet} * \sin(\frac{\pi}{2 * P_{musTi}} * t) & \text{if } 0 < t \leq t_{P_{musTi}} (1) \\ P_{musSet} * \sin(\frac{\pi(t+t_{deflate}-2*t_{insp})}{2*(t_{deflate}-t_{insp})}) & \text{if } t_{insp} < t \leq t_{deflate} (2) \\ 0 & \text{if } t_{deflate} < t \leq TCT (3) \end{cases} \quad (6.3)$$

Eq 6.3 is derived from [Vicario et al., 2015], and consists of 3 phases.

1. The inspiratory phase has a period of $\frac{\pi}{2}$. When $t = P_{musTi}$, P_{mus} reaches the set level.
2. The expiratory phase has a period of $\frac{\pi}{2}$. $t_{deflate}$ is assumed to always be shorter than t_{insp} - thus, P_{mus} will decrease as it reaches 0.
3. In the third phase, P_{mus} is 0 until the beginning of the next respiratory cycle.

6.1.3 Differential Equations for Simulating the Respiratory System

The governing equations of the respiratory module, are implemented as a set of differential equations derived from the EOM.

As depicted in figure H.0.1, the part of the respiratory module comprising the system of equations, can be described by the pseudocode in listing 6.1:

Listing 6.1: Pseudocode for the respiratory model

```

1  for dt in TCT
2      1. Pmus = Pmusdriver
3      2. Calc dPmus
4      3. Pvent = Pventdriver(t)
5      4. Calc flow(t)
6      5. Calc dV
7      6. Calc dPao
8      7. Calc dPpl
9  end

```

Eq 6.4 describes how change in P_{mus} is calculated

$$\Delta P_{mus} = P_{mus}(t) - P_{mus}(t - 1) \quad (6.4)$$

In eq. (6.4), ΔP_{mus} is calculated by the output of the P_{mus} driver function at $t-1$ subtracted from the output at t .

The change in flow at Δt is described in eq. (6.5)

$$flow = \frac{P_{ao}(t) - P_{pl}(t)}{R_{aw}} \quad (6.5)$$

Similar to electron flow in an electrical circuit, eq. (6.5) describes how airflow is calculated as the pressure difference between two nodes over a resistance. In the case of the airways, the first node is P_{ao} , the second node is P_{pl} , and resistance is R_{aw} .

The change in V at Δt is described in eq. (6.6).

$$\Delta V = flow * \Delta t \quad (6.6)$$

The relationship described in eq. (6.6), is derived from the knowledge that volume is the definite integral over flow duration, as described in eq. (6.7).

$$V_t = \int_{start\dot{V}}^{end\dot{V}} \dot{V} dt \quad (6.7)$$

Thus, flow can be expressed as the derivative of V as described in eq. (6.8), from which eq. (6.6) is derived.

$$\dot{V} = \frac{\Delta V}{\Delta T} \Rightarrow \Delta V = \dot{V} * \Delta t \quad (6.8)$$

Change in P_{ao} at Δt is described in eq. (6.9).

$$\Delta P_{ao} = \frac{\Delta V}{C_{rs}} \quad (6.9)$$

This relationship is derived from the fact that $C = \frac{\Delta V}{\Delta P}$. Since C_{rs} has been estimated from the patient data prior to model simulation, and V has been calculated, P_{ao} can be calculated as described in eq. (6.9).

Change in P_{pl} at Δt is described by eq. (6.11)

$$\Delta P_{pl} = \frac{\Delta V}{C_w} + \Delta P_{mus} + \Delta P_{ao} \quad (6.10)$$

This relationship is derived from the EOM, and originally described as eq. (6.11) in Mauri et al. [2017].

$$P_{mus} = \frac{\Delta V}{C_w} - \Delta P_{es} \quad (6.11)$$

Eq 6.9 has been rearranged from eq. (6.11) to output P_{pl} , and assumes that P_{es} can be substituted for P_{pl} .

6.2 Intrathoracic Pressure Module

The purpose of the intrathoracic pressure module, is to simulate the effect of P_{pl} on P_{it} .

As described in section 2.5, changes in P_{pl} are transduced to changes in P_{it} , which change the transmural pressures affecting the cardiovascular system.

6.2.1 Equations

The equation underlying the intrathoracic pressure module is described in eq. (6.12)

$$P_{it} = P_{pl} * \alpha \quad (6.12)$$

It is derived from Cushway et al. [2022] The physiology underlying eq. (6.12), assumes that during transduction from P_{pl} to P_{it} , there will be a pressure loss due to factors such as elasticity of intrathoracic tissue and differing volumes between the pleural cavity and intrathoracic cavity. This pressure loss is described by the factor α .

6.3 Cardiovascular Module

For simulating the cardiovascular system, the CircAdapt cardiovascular simulation framework was implemented. Refer to appendix M for details on CircAdapts anatomy.

CircAdapt is a complex model of the human cardiovascular system. It is first referenced in the scientific literature in 2005 by Arts [2005], and has had major developments in 2012, 2015. [Arts et al., 2012;

Walmsley et al., 2015] It is developed as freeware for use in research, education and engineering. [Team, 2024]

The CircAdapt model is used in several published scientific studies, e.g. Van Osta et al. [<https://doi.org/10.1098/rsta.2019.03>] and Mineroff et al. [2019] for studying cardiovascular related phenomena.

The model consists of a complex system of ordinary differential equations (ODEs), each representing physiological components or functions within the cardiovascular system.

The system is solved using Matlab's `ODE113()`. `ODE113()` is a variable-step, variable-order Adams-Bashforth-Moulton PECE solver. [Matlab, 2023a]

Implementing and adapting CircAdapt for use within the cardiopulmonary model came with advantages and disadvantages, detailed in chapter 8.

6.4 Simulation and Testing Framework

The following section describes the implementation of the framework described in. section 5.1. It consists of a subsection for each module, describing the algorithms with which the respiratory, intrathoracic and cardiovascular module simulate the patient data, respectively. This section concludes with a description of the implemented testing framework.

6.4.1 Respiratory Simulation Algorithm

The first process in the testing framework, is an extraction of the parameters necessary to model the patient's breathing mechanics.

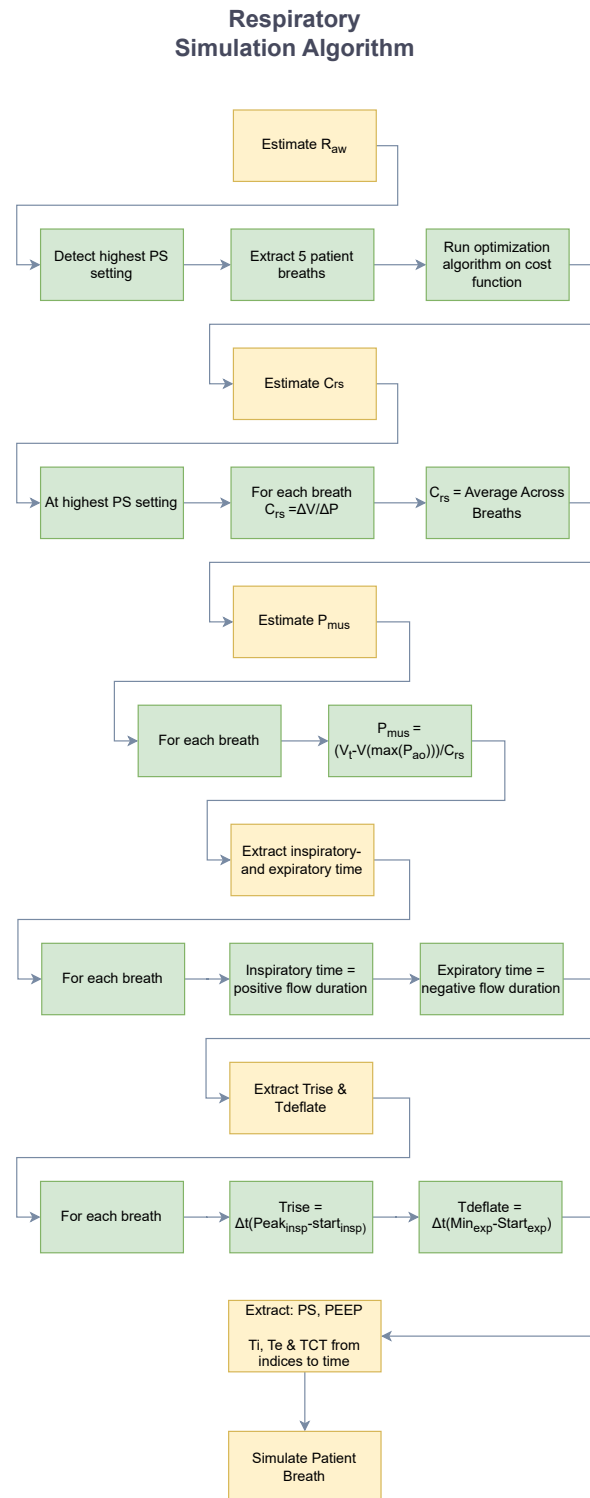


Figure 6.1: The respiratory simulation algorithm in the prediction framework, consists of 7 steps, each with their individual sub-processes.

As seen in figure 6.1, deriving the parameters necessary to simulate the patient's respiratory mechanics, is a 6 step process.

6.4.1.1 Step 1 - Estimate R_{aw}

Estimating the patient's R_{aw} is performed via constrained optimization on a weighted least-squares cost function, described in eq. (6.13)

$$j = \frac{(P_{ao} - \frac{V_t}{C_{rs}} + R_{aw} * flow)^2}{std(P_{ao})} \quad (6.13)$$

Eq 6.13 is derived from the EOM, and assumes no respiratory muscle activity at highest PS settings. P_{ao} , V_t , C_{rs} and flow are available through derivation from the patient's data, and thus R_{aw} is the only unknown.

The optimization is run on 5 patient breaths, and R_{aw} is set as the average R_{aw} across these breaths.

6.4.1.2 Step 2 - Estimate C_{rs}

C_{rs} estimation also assumes no respiratory muscle activity at highest PS settings.

At every breath in the part of the clinical trial where PS is at the highest level, C_{rs} is calculated via eq. (6.14)

$$C_{rs} = \frac{\Delta V}{\Delta P} \quad (6.14)$$

The average C_{rs} across every breath in the timeframe, is assumed to be the patient's true C_{rs} .

6.4.1.3 Step 3 - Estimate P_{mus}

P_{mus} is estimated at every breath in the patient's clinical trial data. The formula for P_{mus} estimation is described in eq. (6.15)

$$P_{mus} = \frac{V_t - (P_{aopeak} * C_{rs})}{C_{rs}} \quad (6.15)$$

The assumption underlying eq. (6.15) is based on the problem statement. Assuming that C_{rs} is the true compliance, we can determine which fraction of V_t corresponds to inflation by P_{vent} as well as P_{mus} .

Thus, $P_{aopeak} * C_{rs}$ equals volume expansion due to P_{vent} , and the remaining V_t must be due to P_{mus} .

6.4.1.4 Step 4 - Extract Inspiratory & Expiratory time

Per convention, inspiratory flow is positive and expiratory flow is negative [Hess R., 2014]. Thus, the inspiratory and expiratory time of each patient breath is derived, by extracting the length at which the corresponding flow values occur.

The extraction algorithm uses a three-point method for determining beginning and end of the respiratory cycle.

First, peaks are detected via matlabs `findpeak()` function. Once peaks have been detected, inspiratory and expiratory time are extracted.

The pseudocode for this algorithm is described below:

```

1  for $peak peaks$
2      % Set three-point indices
3      start_{peak} = peaks(peak)
4      mid_{peak} = peaks(peak+1)
5      end_{peak} = peaks(peak+2)
6
7      % find minimum between peaks
8      min_1 = min(start_{peak}:mid_{peak})
9      min_2 = min(mid_{peak}:end_{peak})
10
11
12     % insp_{length}
13     insp_{length} = flow(min_1:min_2)>0
14     % exp_{length}
15     exp_{length} = flow(mid_{peak}:end_{peak})<0
16
17 end

```

This algorithm is visualized in section 6.4.1.4

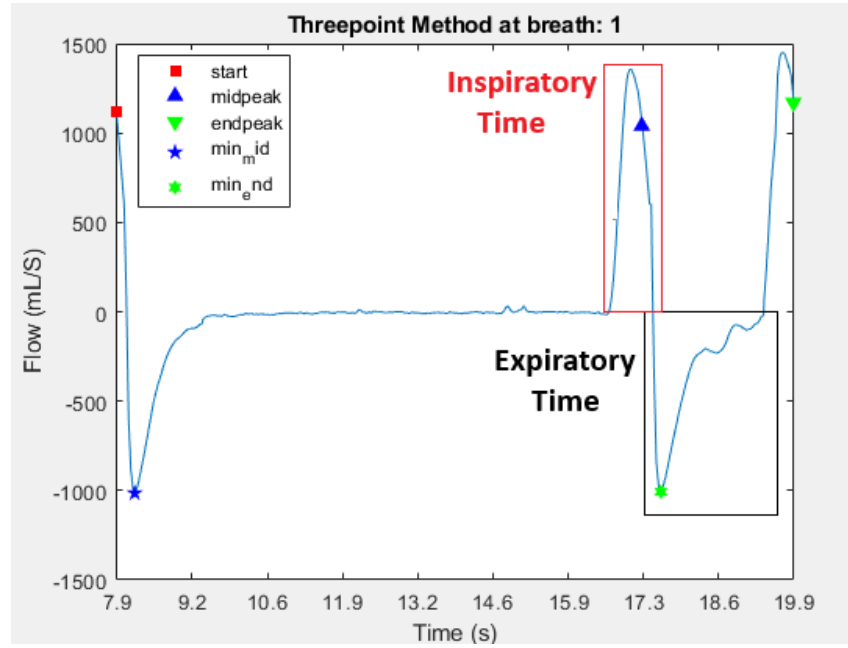


Figure 6.2: Visualized process of inspiratory- and expiratory time extraction. Inspiratory time corresponds to all indices between min_{mid} and $min_{end} > 0$. Expiratory time corresponds to all indices between midpeak and endpeak < 0 .

6.4.1.5 Step 5 - Risetime and Deflation Time

Through the inspiratory and expiratory times derived in section 6.4.1.4, the T_{rise} and $T_{Deflate}$ are extracted.

As visualized in figure 6.3, T_{rise} consists of the indices from start of breath until $insp_{flowpeak}$. $T_{deflate}$ consists the indices from start of expiratory flow, until $flow_{min}$.

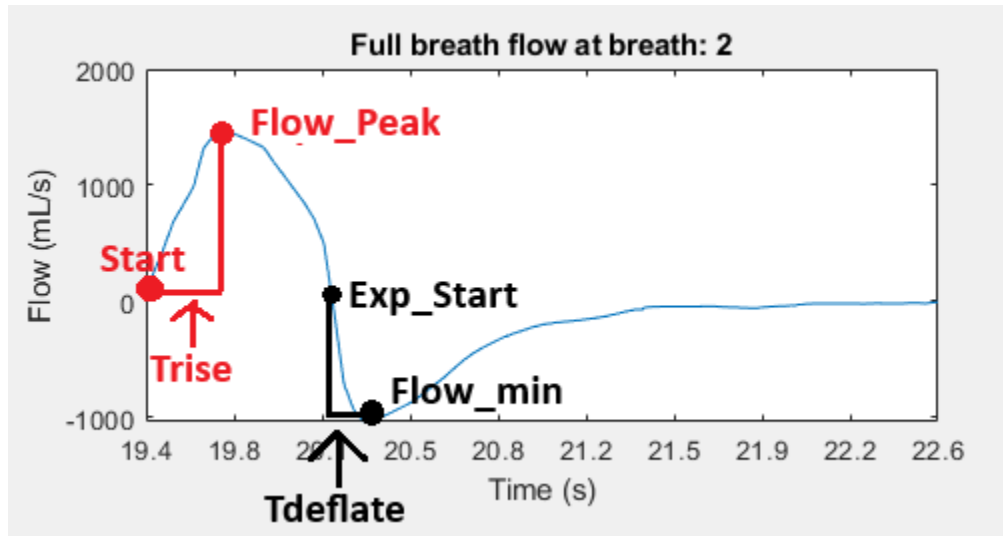


Figure 6.3: Extraction of T_{rise} and $T_{deflate}$. The time from beginning of breath until $insp_{flowpeak}$ constitutes T_{rise} . $T_{deflate}$ is found from $flow = 0$ until $exp_{flowmin}$

6.4.1.6 Step 6 - Remaining Input Extraction and Breath Simulation

In the last step of the respiratory simulation algorithm, PS and PEEP are extracted from the patient's data, and T_i , T_e , TCT , T_{rise} and $T_{deflate}$ are converted from indices to seconds.

The extracted parameters and inputs are then given as arguments to the respiratory module.

Lastly, the patient's breath will be simulated as described in section 6.1

6.4.2 Pulse Pressure Variation Simulation Algorithm

Once the patient's breath has been simulated as described in section 6.4.1, PPV simulation commences.

In order to simulate PPV, the algorithm first simulates the cardiovascular system, after which the cardiopulmonary interactions are simulated.

Fig 6.4 visualizes the flowchart of the PPV simulation algorithm, describing the performed steps and sub-processes.

6.4.2.1 Simulate Cardiovascular System

The cardiovascular system is modelled for the timeframe being studied, via the CircAdapt cardiovascular system module described in appendix M.

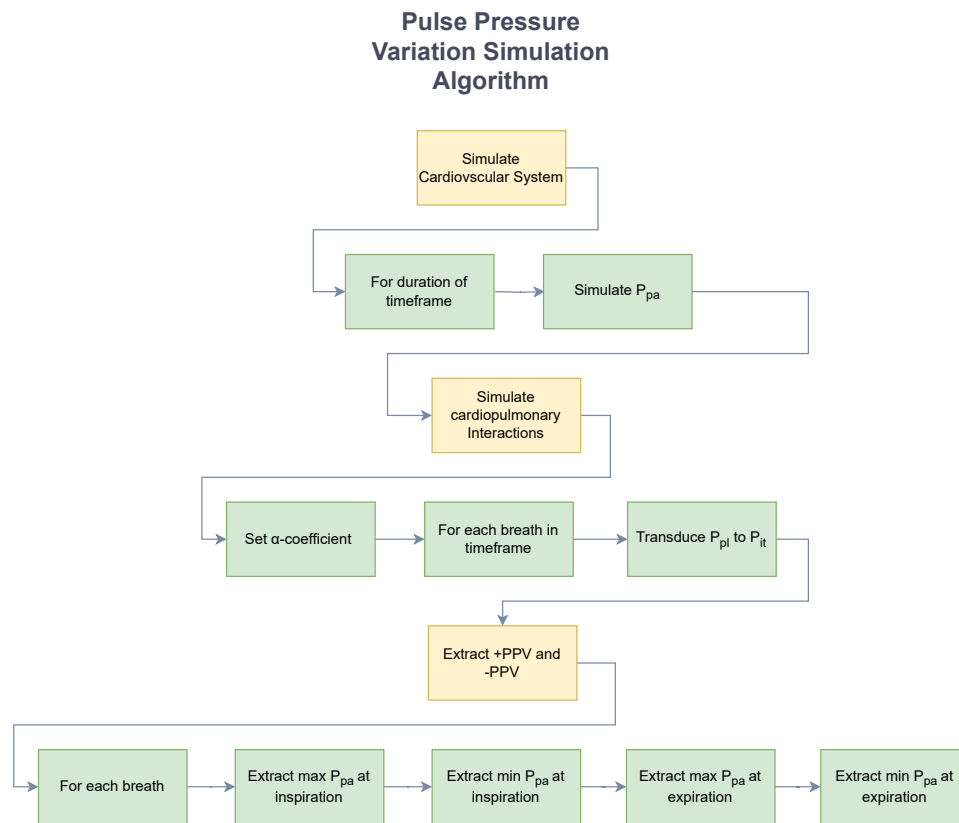


Figure 6.4: The Pulse Pressure Variation Simulation Algorithm of the prediction framework. The algorithm consists of 7 steps, each with their individual sub-processes.

The model has been modified to disregard the effects of transpulmonary pressures. These will, thus, be reinstated in synchrony with the patient's breathing patterns, via the intrathoracic module.

6.4.2.2 Simulate Cardiopulmonary Interactions

Once the patient's breathing patterns as well as cardiovascular system have been modelled, the intrathoracic module, described in section 6.2, models the cardiopulmonary interactions.

Listing 6.2 describes the pseudocode by which the cardiopulmonary interactions are modelled

Listing 6.2: Pseudocode for cardiopulmonary interactions simulation

```

1  for timeframe
2      for breath in timeframe
3          synchronize breath index with timeframe
4
5          transduce Ppl to Pit via intrathoracic module
6      end
7  end

```

Fig 6.5 shows an example of the simulation of P_{pa} within the cardiovascular system, prior to simulation of cardiopulmonary interactions.

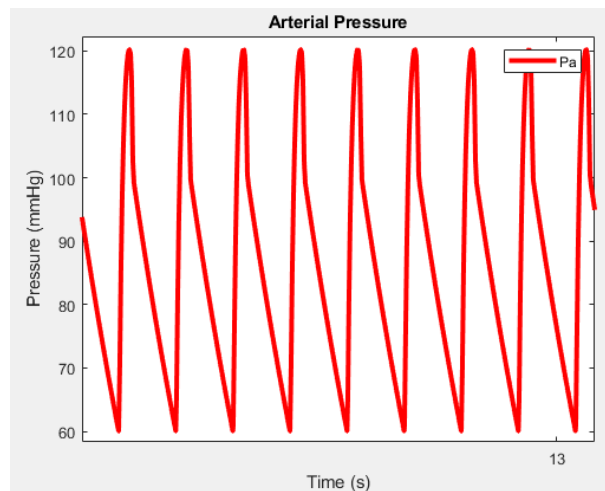


Figure 6.5: Example of P_{pa} simulated prior to simulation of cardiopulmonary interactions

6.6 shows an example of the simulation of P_{pa} within the cardiovascular system, after the simulation of

the cardiopulmonary interactions.

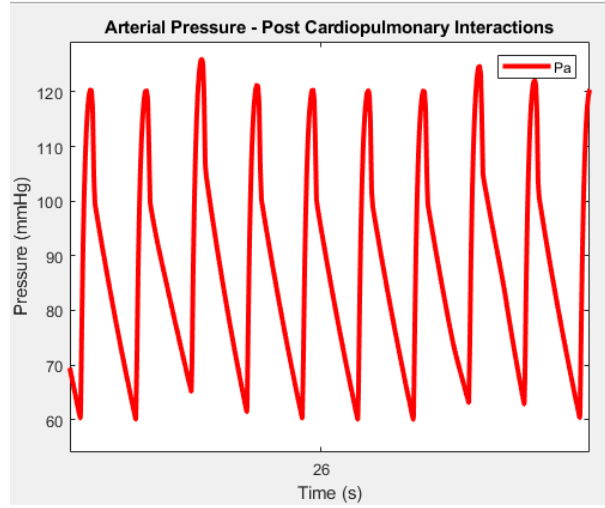


Figure 6.6: Example of P_{pa} simulated with cardiopulmonary interactions.

6.4.2.3 Step 6 - Extract +PPV/-PPV

As described in section 2.6.2, an assumption regarding the delineation of PPV as a result of P_{mus} and PS can be made.

In order to model this assumption, peaks are detected during the inspiratory- and expiratory phases of the respiratory cycle. These peaks correspond to the systolic pressures during the time intervals. The peaks are then marked according to min and max P_{pa} during inspiration- and expiration respectively.

To distinguish these measurements, they are termed +PPV/-PPV, calculated as described in eq. (6.16) and eq. (6.17)

$$+PPV = Max_{insp} - Min_{exp} \quad (6.16)$$

$$-PPV = Max_{exp} - Min_{insp} \quad (6.17)$$

The extraction algorithm is visualized in figure 6.7.

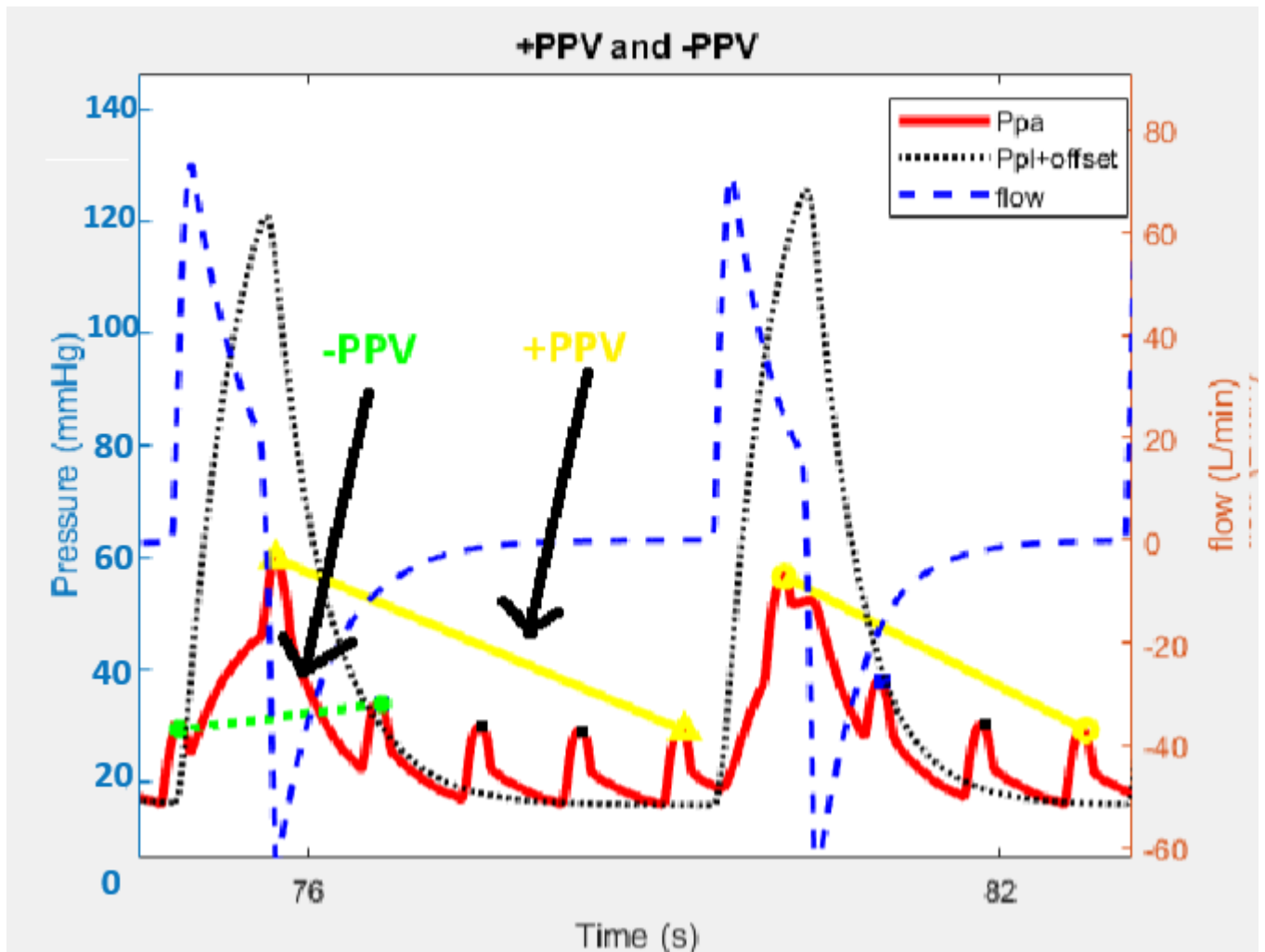


Figure 6.7: Visualization of the +PPV/-PPV extraction algorithm. +PPV is represented by the solid yellow line, showing the connection between Max_{insp} and Min_{exp} . -PPV is represented by the green dotted line, showing the connection between Min_{insp} and Max_{exp} .

6.4.3 Compare results

When the process described in section 6.4.1 has concluded, all parameters and inputs for model simulation will have been extracted. Thus, comparison between the PPV values estimated by the model and PPV extracted from the patient's data can be conducted.

This process, visualized in figure 6.8 incorporates two statistical tools for determining efficacy between measurement methods. These tools are the Bland-Altman plot and a coefficient of determination.

Statistical Comparisons

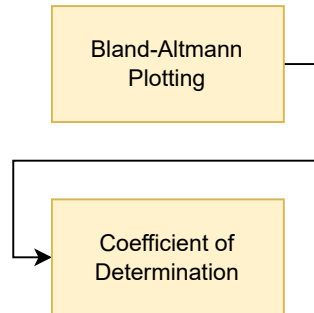


Figure 6.8: The comparison of results process, consisting of the Bland-Altman Plotting & Coefficient of Determination steps.

Bland-Altman Plotting Bland-Altman plots are a tool for comparing how well two methods of measurement correlate with each other.

The method was introduced in Bland and Altman [1986], and has since widely been used in the field of medicine.

Bland-Altman plots provide insight into the data, by visualizing the mean differences at each measurement point. The Bland-Altman plot incorporates the limits of agreement (LOA), being ± 1.96 standard deviations, allowing for conclusions on expected deviations of the measurements. This way, the Bland-Altman plot can easily detect outliers and systematic measurement trends, providing insight into the data.

Since Bland-Altman plots assume normality, all samples were tested for normality with Matlab's `kstest()` function. [Matlab, 2023b]

6.4.3.1 Coefficient of Determination

The coefficient of determination (R^2) is a second method for evaluating the problem statement. Whereas Bland-Altman plotting provides a way to compare the two methods in a number of ways described above, the output of the R^2 provides evaluation as a single integer.

The R^2 is described in eq. (6.18)

$$R^2 = 1 - \frac{SSR}{\sum_{n=1}^N (SS_{total})} \quad (6.18)$$

Where the sum of squared residuals (SSR) is divided by total sum of squares (SS_{total}).

6.5 Parameter Optimization Framework

In order to estimate the optimal parameters for the model, an optimization framework was build. The flowchart for the parameter optimization framework is visualized in figure 6.9.

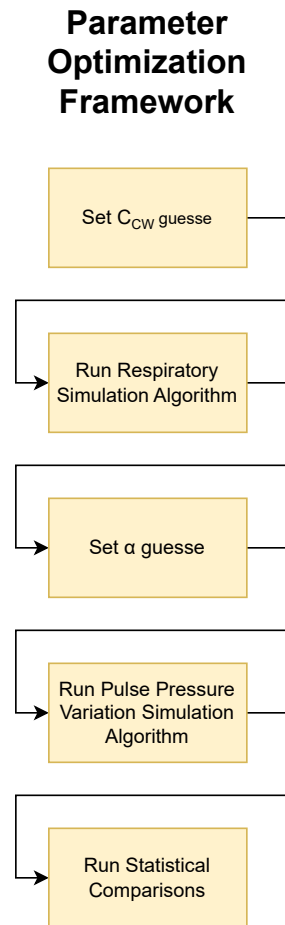


Figure 6.9: Flowchart for the parameter optimization framework. The framework combines the previously described algorithms, and runs them in sequence with variations of C_{cw} and α . The combination of C_{cw} and α yielding the highest R^2

The framework estimates combination of C_{cw} and α . It then evaluates the combination with the highest

R^2 , as well as the lowest mean difference between measurements.

7 | Results

7.1 System Requirement Testing

In the following section, the results from the system requirement testing will be presented. Each subsection will have a reference to the relevant test protocols.

7.1.1 SR02 + SR03 + SR04

Refer to appendix E for the test protocol.

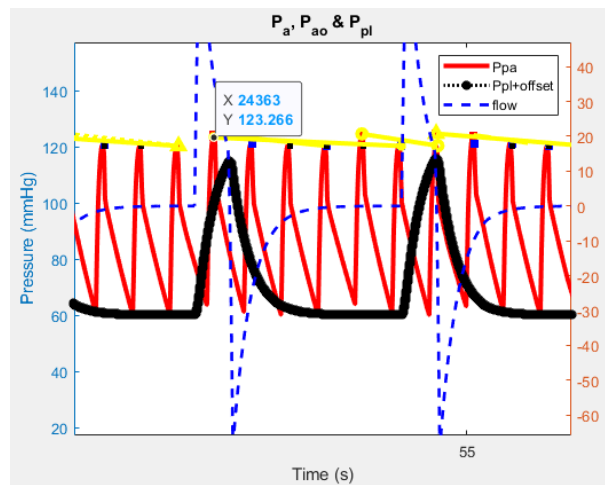


Figure 7.1: Graph visualizing the highlighted test point. Note that P_{pl} has been vertically shifted by an offset and scaled.

P_{pa} Baseline	151.78 mmHg
P_{pl}	4.29 mmHg
P_{it} ($P_{pl} * 0.55$)	2.26 mmHg
P_{pa} Post-Processing	123.27 mmHg

Table 7.1: Values of test variables defined in appendix E

Test Status: Success

7.1.2 SR05

Refer to appendix F for the test protocol

Fig 7.2 shows an example of a permutation performed during the testing. This example demonstrates

SB simulated by the model. The most notable input is T_i , has been modified to 0.75S in order to more closely model patient 2's data at the first timeframe.

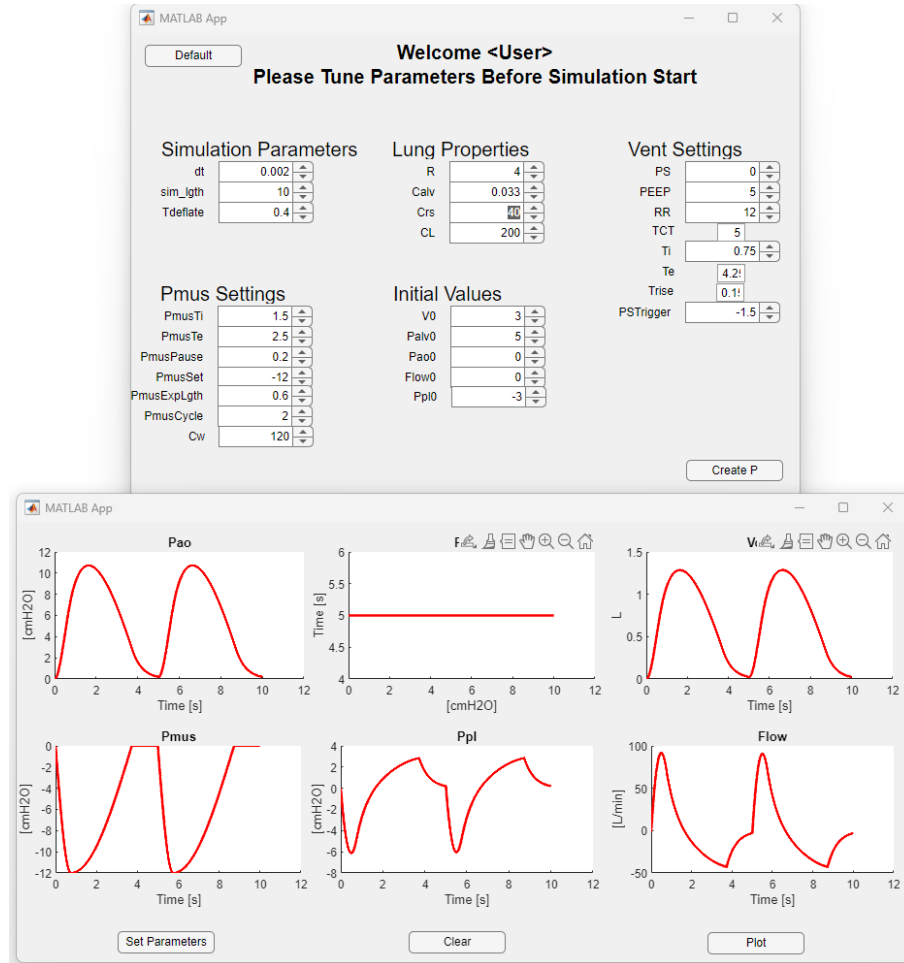


Figure 7.2: Example permutation performed during testing. This simulation is dominated by SB, as PS is 0. T_i has been set to 0.75S, in order to simulate the patient 2's breathing pattern during the first timeframe. As a result, T_e is 4,25S, as the model calculates T_e by subtracting T_i from RR.

Test Status: Succes

7.1.3 SR06

Refer to appendix G for the test protocol

Figure 7.3 and figure 7.4 show 2 examples of permutations performed during testing.

In figure 7.3 The model is set to simulate a high PS level, which is present during the first timeframes of

patient 2's trial.

Most notably, the test is set to simulate a PS setting of 20, PmusCycle of $2 \frac{L}{min}$ and PmusSet of -12 cmH_2O , whereas

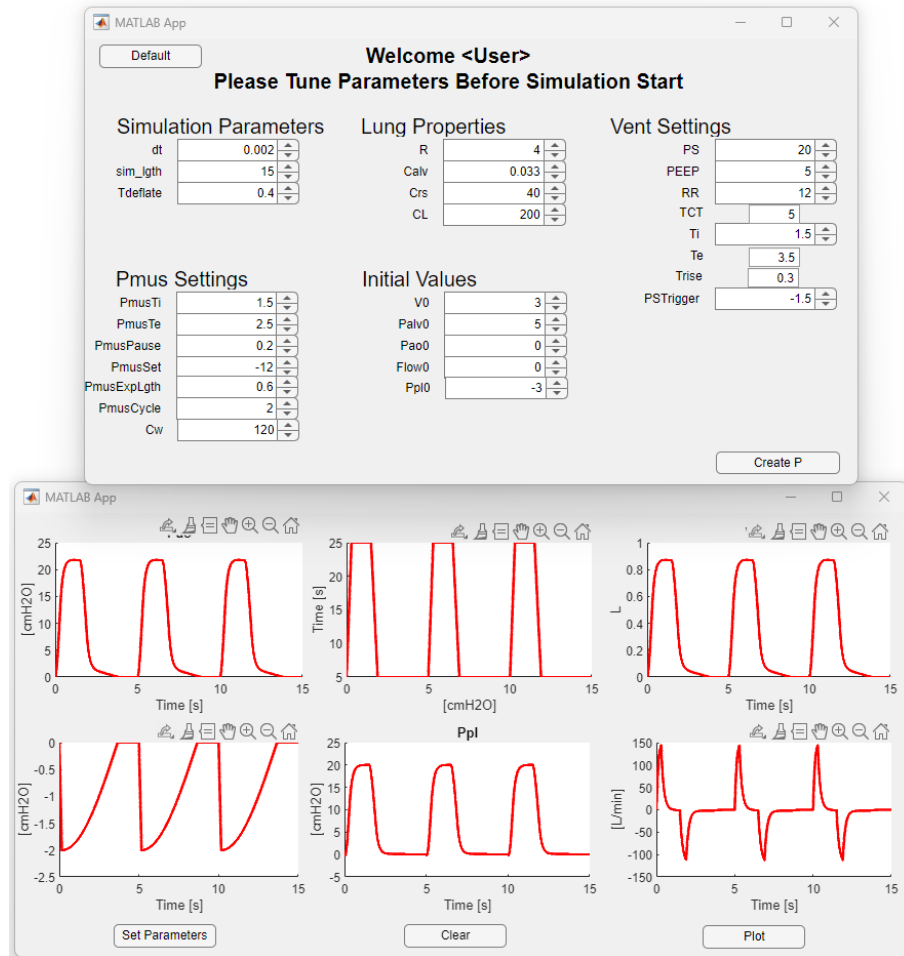


Figure 7.3: An example of a permutation performed during the testing phase. The model has been set to simulate high PS levels. Most notably, a PS setting of 20, PmusCycle of $2 \frac{L}{min}$ and PmusSet of -12 cmH_2O is shown.

Figure 7.4 shows another example of a permutation performed during the testing phase. Compared to figure 7.3, PS has been set to 12 cmH_2O , in order to see the model's behavior when PS is close to PmusSet.

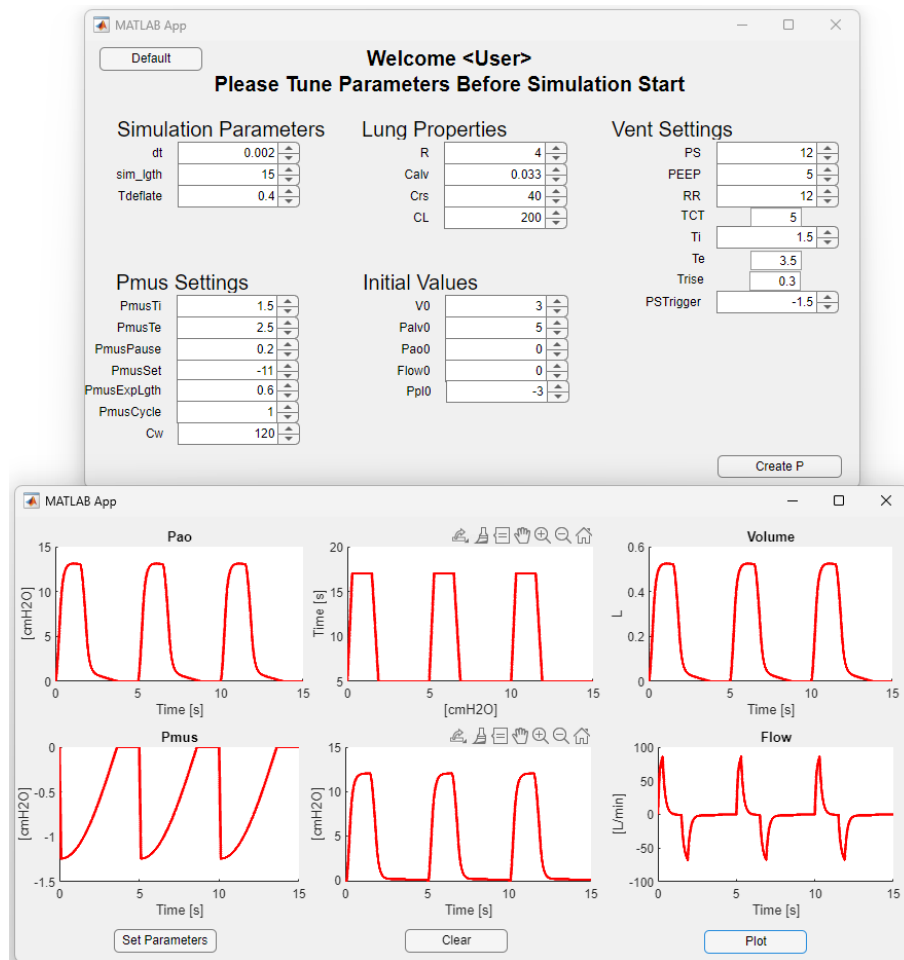


Figure 7.4: Another example of a permutation performed during the testing phase. PS has been set to 12, in order to test the models behavior when PS is close to PmusSet.

7.2 Individual Chunk Results

In order to diagnose the models performance at each timeframe of the clinical trial data, each timechunk was individually examined. This analysis yielded insight into the models ability to predict +PPV/-PPV at different PS levels.

App N contains the results for the models performance on predicting +PPV/-PPV. Furthermore, testing was conducted on the models ability to predict $P_{insp_{max}} - P_{exp_{min}}$, as well as $P_{insp_{min}} - P_{exp_{max}}$, in order to diagnose where performance improvements could be identified.

The results of the individual chunk diagnosis indicated that the model had significantly lower accuracy

at $PS = 3.1$ and $PS = 2.1$. Thus, the performance of the model of the entirety of the patient data was tested with and without these chunks. See appendix N.0.4 for excluded results.

7.3 Full Patient Data

7.3.1 Patient 2

Following the analysis of each individual timeframe within patient 2's clinical trial, the model was tested on its ability to predict +PPV/-PPV on timechunks 1-16 of the patient data.

Fig 7.5 shows the models performance on timechunks 1-16, constituting a total of 595 breaths.

Through the optimization framework described in section 6.5, the combination of C_{cw} and α yielding the best performance on R^2 and $\Delta mean$ were detected.

+PPV

Fig 7.5 A) shows +PPV predictions.

For +PPV, the simulations resulted in $R^2 = 0.19$, and a $\Delta mean$ between simulated and measured measurements of -0.176%.

The residual plots show a clustering round the regression line at, which disperses as +PPV gets higher. This indicates a trend to predict +PPV with high precision at lower percentages, but increase in prediction error as percentages get higher. Furthermore, the residual plot shows a tendency for the model to evenly over- and underestimate +PPV.

The Bland-Altman Plot shows the normal distribution of the data, with a heavy clustering +/- 1STD around the mean, an expected amount of observations laying within the limits of agreement (LOA), and 2.5% (15) of the observations are beyond the positive and negative LOA. The observations are evenly over- and underestimated, conforming the trends of the residual plots.

A $\Delta mean$ of -0.176% indicates that the model predicts +PPV on average, with a slight tendency for underestimation.

-PPV

Fig 7.5 b) shows -PPV predictions.

For -PPV, the simulation resulted in $R^2 = 0.01$ and a $\Delta mean$ between simulated and measured -PPV of

-0.152%.

The R^2 indicates that the regression model was not a good fit. However, the residual plots shows a more evenly horizontal distribution around the regression line than +PPV. The observations cluster between measured -PPV of 0-1.8%, indicating that the model performs most accurately at these percentages. The clustering disperses at lower and higher -PPV, indicating a similar trend to +PPV.

The Bland-Altman plot shows a normal distribution of the data. 6.3% (38) of the observations are beyond the positive and negative LOA, indicating that the has a lower accuracy when predicting -PPV.

A $\Delta mean$ of -0.153% indicates that the model predicts -PPV on average, with a slight tendency for underestimation.

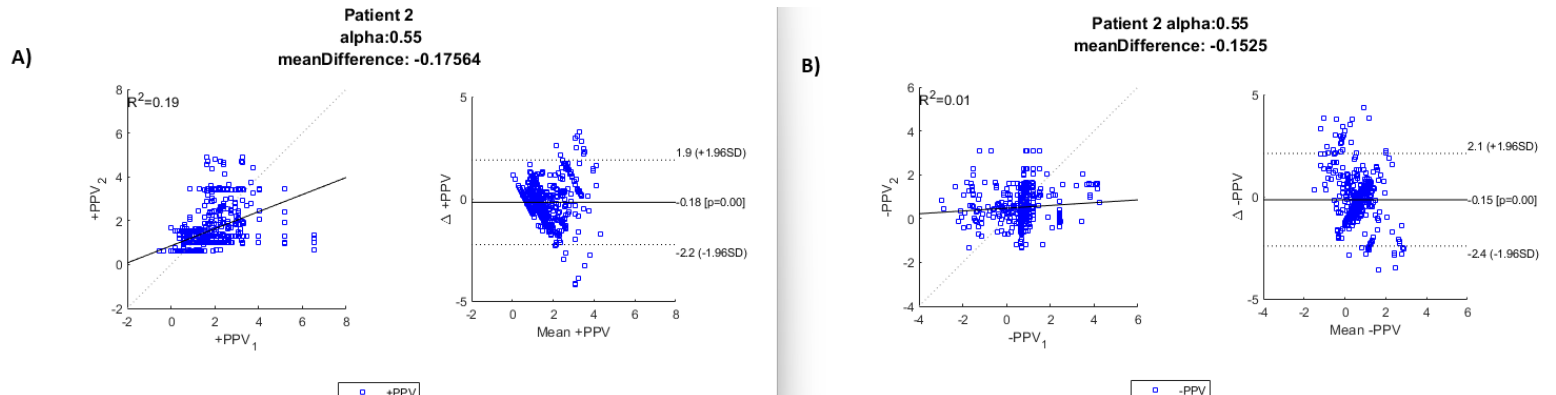


Figure 7.5: A) +PPV B) -PPV for patient 2. In **A)** the residual plots indicate a trend to predict +PPV with high precision at lower percentages, and a tendency to evenly under- and overestimate +PPV. The Bland-Altman plot in **A)** shows a normal distribution of the data, confirming the trends of the residual plots. With a $\Delta mean$ of -0.176%, +PPV is predicted with slight underestimation on average. In **B)**, a more even horizontal distribution around the regression line is shown. A cluster is centered around 0-1.8%, dispersing at higher and lower -PPV. This indicates a similar trend to +PPV. The Bland-Altman plot shows -PPV to be normally distributed though there are more outliers than +PPV. With a $\Delta mean$ of -0.153%, -PPV is predicted with slight underestimation on average.

7.3.2 Patient 3

Fig 7.6 shows the model's performance on patient 3's clinical trial data.

The dataset consists of 6 timechunks, constituting a total of 3464 breaths.

The optimization framework yielded the best performance at α 0.7.

+PPV

Fig 7.6 A) shows +PPV predictions.

For +PPV, the simulations resulted in $R^2 = 0.62$ and a $\Delta mean$ of 0.53%.

The residual plots shows a close fit around the regression line at negative predicted +PPV. Then, a clustering centered slightly above 0, followed by a vertical rise. This shows a trend of high accuracy when +PPV is negative, average accuracy at percentages between 0-7.5%, and reduced accuracy as predicted percentages rise.

The full graph appears to have low variance. Fig figure 7.7 shows a zoomed graph, highlighting the variance within the dataset.

The Bland-Altman plot shows a normal distribution of the dataset. A total of 77 observations fall beyond the LOA, with 1.96% (68 observations) above the positive- and 0.26% (9 observations) below the negative- LOA. 40.12% (1391 observations) fall within the positive- and 57.68% (1998) within the negative- LOA. This indicates indicates a tendency for the model to overestimate observations.

With a $\Delta mean$ of 0.53%, the model predicts +PPV accurately on average.

-PPV

Fig 7.6 B) shows -PPV predictions.

For -PPV, the simulations resulted in $R^2 = 0.04$ and a $\Delta mean$ of 3.35%.

The residual plots show a horizontal fit on the regression line. This indicates that the model systematically predicts with the same accuracy.

The Bland-Altman plot shows a normal distribution of data dataset. A total of 188 observations fall beyond the LOA, with 5.2% (180 observations) above the positive- and 0.23% (8 observations) below the negative- LOA. 83% (2874 observations) fall within the negative- and 11.6% (402 observations) within

the positive LOA. This indicates a tendency for the model to overestimate observations.

A $\Delta mean$ of 3.3466%, the model vastly overestimate PPV on average.

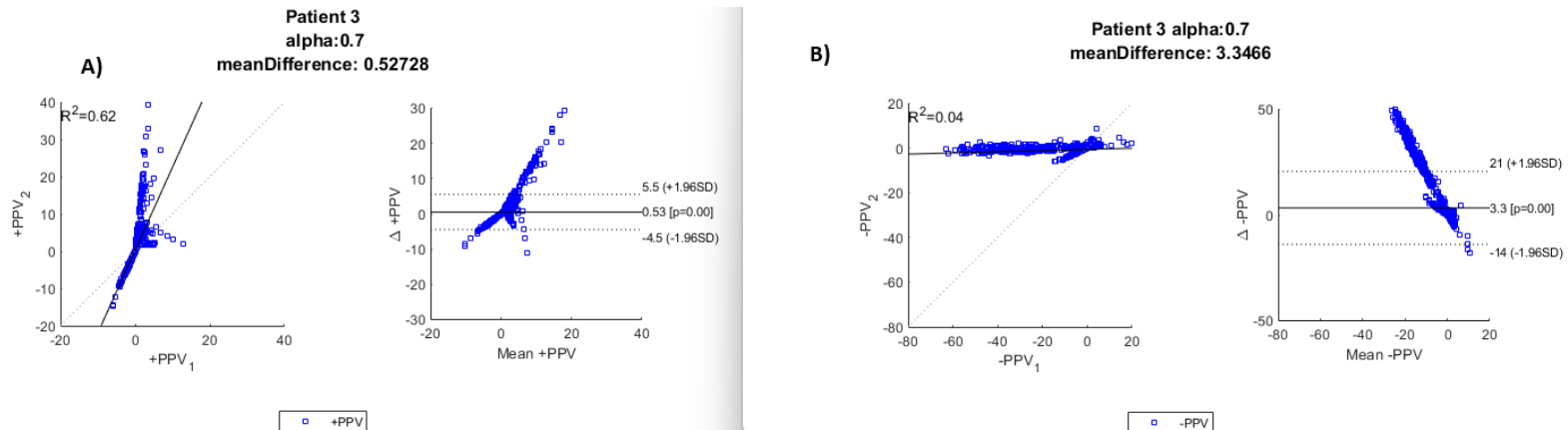


Figure 7.6: A) +PPV B) -PPV for patient 3. In **A)** the residual plots show a trend of high accuracy at negative $+PPV$, average accuracy between 0-7.5%, with accuracy reducing above. The Bland-Altman plot shows a normal distribution. A total of 2.22% of observations are statistical outliers. The majority of observations falling between 0 and -1.96STD, indicate the model's tendency to overestimate observations. A $\Delta mean$ of 0.53% indicates accurate predictions on average. In **B)** the residual plots show that the model systematically predicts with the same accuracy. The Bland-Altman plot shows a normal distribution. A total of 5.43% observations are statistical outliers. The majority of observations falling between 0 and -1.96STD indicates a tendency for the model to overestimate observations. $\Delta mean$ if 3.35% show a trend of vastly overestimating on average.

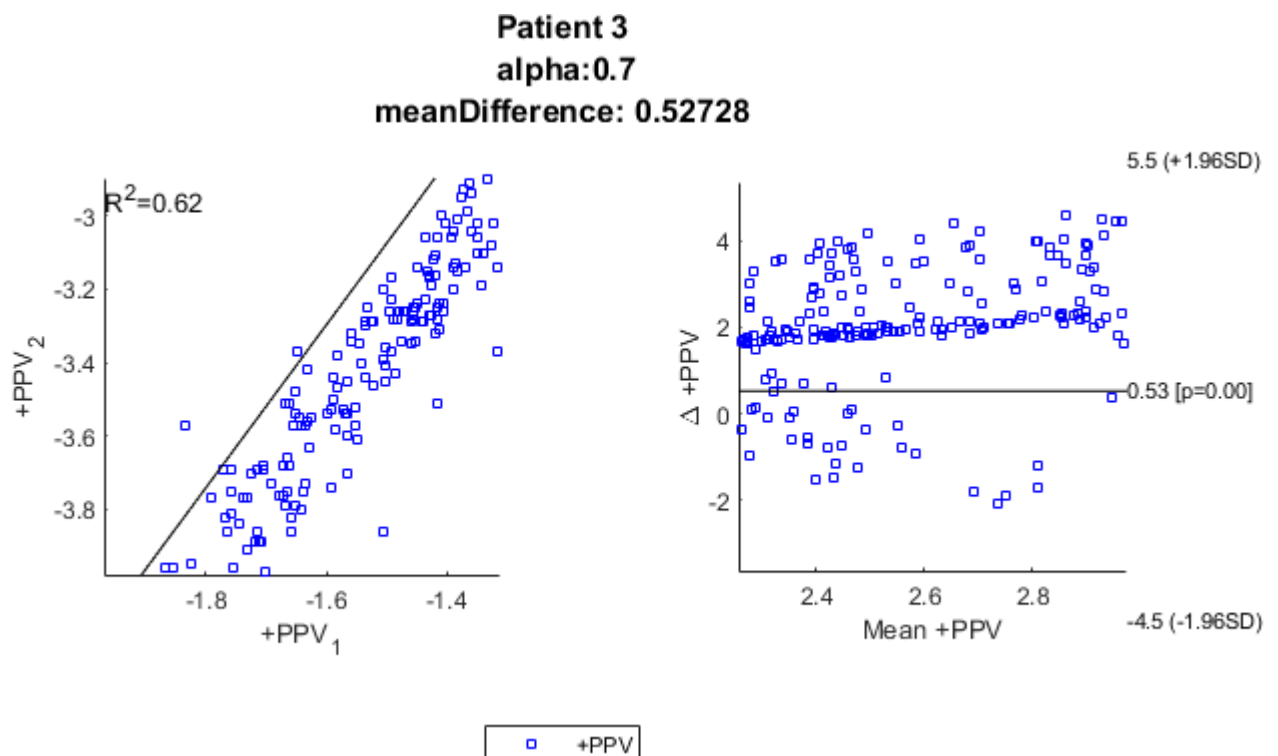


Figure 7.7: Caption

8 | Discussion

As described in section 2.5, cardiopulmonary interactions are a result of the variations in P_{it} which occur during the respiratory cycle. Thus, during the inspiratory phase of PPVENT the transmural pressures within the cardiovascular system decrease, and during the expiratory phase they increase. The change in transmural pressure in response to the respiratory phase is reversed during NPVENT, such as which occurs during SB. [Pinsky, 2017; Feher, 2017]

The cardiopulmonary interactions add a second signal to P_a , which correspondingly increases and decreases in response to the varying transpulmonary pressures. This signal allows for the extraction of PPV, which quantifies the change in P_a resulting from cardiopulmonary interactions [Trebloul et al., 2018]. Eq 8.1 describes the calculation of PPV:

$$PPV = \frac{P_{pamax} - P_{pamin}}{(P_{pamax} - P_{pamin}) * 0.5} * 100 \quad (8.1)$$

PPV can be used as a biomarker for FR, as described in section 2.5.4. The underlying hypothesis for PPV as a biomarker for FR, is that large respiratory changes to LV SV occur when the patient is biventricular preload responsive. [Trebloul et al., 2018]

The aim of this project was to design and implement a physiological model, capable of supporting in-silico experimentation of the projects hypothesis. In-silico experimentation utilizes the advantages described in section 2.4. The projects hypothesis states that "PPV can be used to estimate FR during conditions where SB occurs, by combining +PPV/-PPV at the highest and lowest PS settings". The underlying theory for the hypothesis is described in section 2.7.

Based on the problem analysis and hypothesis, the projects problem statement was formulated:

"How can a computational model be designed and implemented, to predict +PPV/-PPV in pressure support mechanically ventilated patients?"

The technical solution to the problem statement, led to the development of a model capable of simulating cardiopulmonary interactions. The model predicted +PPV on the test subjects with respectively $R^2 = 0.19$ and $R^2 = 0.62$, with a mean difference between predicted and measured +PPV at respectively -0.176% and 0.53%. In patient 2, a Bland-Altman plot analysis showed the observations to be normally distributed. Both the residual- and Bland-Altman plots showed the models predictions to be accurate

on average, with a slight tendency for overestimation. Only 2.5% of +PPV predictions were statistical outliers, supporting the accuracy of the model. In patient 3, normal distribution was observed. 2.22% of observations were outliers, 97.78% were within the LOA, with 57.68% being within the negative- and 40.12 within the positive LOA.

In patient 2, the model's prediction of -PPV resulted in an $R^2 = 0.01$ and a mean difference between predicted and measured -PPV at -0.153%. The residual plot indicates that -PPV is predicted most accurately between 0-1.8%. The Bland-Altman plot showed a normal distribution of the predictions. A mean difference of -0.153%, -PPV predictions were accurate on average, with a slight tendency for underestimation. With 6.3% of the data being statistical outliers, indicating that -PPV has a higher total prediction error. In patient 3, the simulation resulted in an $R^2 = 0.04$, and a Δ_{mean} of 3.35%. With 83% of observations falling within the negative LOA, the trend shows a tendency to overestimate observations.

The results from the test show, that model's performance is vastly more accurate when predicting +PPV than -PPV. This is further amplified by the fact that the model tends to overestimate observations, yielding better results at positive values. App N shows a tendency for the models prediction to be more precise when higher PS settings are present, and less precise the lower PS setting is applied. The combination of this analysis, indicates that the models PS simulation is more accurate than its SB simulation, and that the P_{pl} has a tendency to be higher than that in the clinical trials.

To the knowledge of the author, no previous studies have attempted to research cardiopulmonary models aimed at predicting +PPV/-PPV. Several studies, such as Albanese et al. [2013] and [Vicario et al., 2015] have researched in-silico modelling of P_{mus} and P_{pl} estimation. Moreover, in-silico modelling of cardiopulmonary interactions has been researched by Cushway et al. [2022]. Therefore, the clinical trial data from which +PPV/-PPV was measured were used as the state-of-the-art benchmark with which to compare the models performance.

The project designed, built and tested a mathematical model capable of simulating the respiratory cycle. The model used the EOM as a foundational mathematical model of the mechanical ventilators interactions with the respiratory systems. The EOM is a common basis for respiratory modelling in the respiratory research community. [Cushway et al., 2022]. Inspired by Vicario et al. [2015], P_{mus} was implemented as a sine-function, with assumptions about monotonistic increase- and decrease during in- and expiration and a respiratory pause. Furthermore, the ventilator was implemented with a driver function, with PS and PEEP governing the pressures, t_{rise} , $t_{deflate}$, t_{insp} and t_{exp} governing the timing and PSTrigger

governing its activation. Before testing on clinical trial data commenced, the respiratory model was tested in a custom-built test setting in a virtual environment for performance evaluation. The model simulated the interactions between the ventilator and respiratory system accurately during test conditions.

The model's performance was tested on patient data as described in section 7.3.1. Due to the nature of the experimental data, every timechunk was analyzed in order to diagnose the model's behavior on varying PS levels. This testing regime led to a detailed understanding of its performance within the clinical trials. However, since the model was only tested on a limited sample size, there is a risk of overfitting, and hence the results not being generalizable. Thus, before the results of the model can be generalized to a larger population of MV patients, the sample size must be expanded.

During the literature search into mathematical modelling of the cardiovascular system, CircAdapt was discovered. CircAdapt is a comprehensive freeware model of the cardiovascular system, designed for scientific, research and engineering usage. [Team, 2024] Due to its usage within research on the cardiovascular system, such as e.g. Van Osta et al. [<https://doi.org/10.1098/rsta.2019.0347>] and Mineroff et al. [2019], it was hypothesised to be of value to this project. As described in ??, CircAdapt was implemented and performed the function of the cardiovascular module. However, the number of parameters combined with its questionable accuracy at single-beat simulations, meant that CircAdapt was not used to its full potential. Despite Circopt, a parameter optimization tool designed for CircAdapt [Mineroff, 2019], being tested to counteract CircAdapt's disadvantages, it never reached a state of patient-specific cardiovascular modelling. Thus, a custom built lumped model of the cardiovascular system would have been a more effective approach, hypothesised to have been easier adaptable to the patient's cardiac rhythm as well as more computationally efficient.

Future perspectives for the work of cardiopulmonary modelling with the aim of predicting +PPV/-PPV should include further work on the respiratory model, the cardiovascular model and improving parameter as well as input extraction.

Improvements to the respiratory model should include an external respiration module, capable of simulating partial pressure of CO_2 (PCO_2) and partial pressure of O_2 (PO_2).

The external respiration module would allow for a sophisticated mechanism improving the timing of respiratory muscles activation at SB. Improvements to the cardiovascular model should include either a custom built lumped heart model, or adaptation of CircAdapt to meet the needs of this project's model.

Parameter and input extraction should be improved by further pre-processing of the data, assuring that

the extraction algorithms extract the desired features with minimal error.

9 | Conclusion

This study presented a method for predicting +PPV/-PPV in mechanically ventilated patients, with the aim of predicting FR, with routinely available respiratory data.

The study's problem statement was as follows

"How can a computational model be designed and implemented, to predict +PPV/-PPV in pressure support mechanically ventilated patients?"

The results of applying the model to clinical trial data, showed that the model's +PPV/-PPV predictions were accurate on average, with tendencies for slight over- and underestimation, respectively. The model showed decent results when predicting +PPV, with $R^2 = 0.63$ in patient 3 and $R^2 = 0.19$ in patient 2. Moreover, the distribution of the Bland-Altman plots showed the models tendency of favoring overestimation, and the analysis of individual timeframes demonstrated lowest accuracy of predictions at timeframes with low PS levels. Thus, the model performed well when predictions involved high P_{it} , and its accuracy fell at lowered P_{it} . This could indicate that the PS module of the model was better at adapting to the patient's physiological state than the SB module.

Testing was performed both on individual timeframes as well as full patient data. However, the testing was performed on a limited sample size. Thus, the sample size should be expanded before the conclusions can be generalized.

The conclusion of the study is:

The combination of the respiratory- cardiovascular- and intrathoracic- model for simulating cardiopulmonary interactions, with the aim of predicting +PPV/-PPV, performed accurately on average. The model performed best when predicting +PPV, and under conditions of high PS, indicating that the PS module was better at adapting to the patient's physiology than the SB module. Thus, improvements to the SB module are hypothesised to improve the cardiopulmonary models +PPV/-PPV predictions. Expanding of the testing sample size is necessary before the conclusions can be generalized.

10 | Bibliography

- Albanese et al., 2013.** A. Albanese, N. Karamolegkos, S. Haider, A. Seiver and N. Chbat. *Real-Time Noninvasive Estimation of Intrapleural Pressure in Mechanically Ventilated patients: A Feasibility Study*. 2013. URL <https://pubmed.ncbi.nlm.nih.gov/24110910/>.
- Arts et al., 2012.** J. Arts, T. and Lumens, W. Kroon and T. Delhaas. *Control of Whole Heart Geometry by Intramyocardial Mechano-Feedback: A Model Study*. 2012. doi: <https://doi.org/10.1371/journal.pcbi.1002369>.
- Arts, 2005.** T. et. al. Arts. *Adaptation to mechanical load determines shape and properties of heart and circulation: the CircAdapt model*. 2005. doi: doi:10.1152/ajpheart.00444.2004.
- Barh et al., 2013.** D. Barh, V. Chaitankar, E. C. Yiannakopoulou, E. O. Salawau, S. Chowbina, P. Ghost and V. Azevedo. *In Silico Models*. 2013. doi: 10.1016/B978-0-12-416002-6.00021-3.
- Bates H. T., 2009.** Jason Bates H. T. *The Linear Single-Compartment Model*. 2009. URL <https://www.cambridge.org/core/books/abs/lung-mechanics/linear-singlecompartment-model/880B7408A8F37FAA4258FE6EE41130BE>.
- Bland and Altman, 1986.** J. Bland and D. Altman. *Statistical methods for assessing agreement between two methods of clinical measurement*. 1986. URL <https://pubmed.ncbi.nlm.nih.gov/2868172/>.
- Carvalho et al.** E.B. Carvalho, D. Battaglini, C. Robba, M. L. N. G. Malbrain, P. Pelosi, P. R. M. Rocco and P. L. Silva. *Fluid management strategies and their interaction with mechanical ventilation: from experimental studies to clinical practice*. URL <https://www.ncbi.nlm.nih.gov/pmc/articles/PMC10359242/>.
- Charalampidis et al., 2015.** C. Charalampidis, A. Youroukou, G. Lazaridis, S. Baka, I. Mpoukovinas, V. Karavasilis, I. Kioumis, G. Pitsiou, A. Papaiwannou, A. Karavergou, K. Tsakiridis, N. Katsikogiannis, E. Sarika, K. Kapanidis, L. Sakkas, I. Korantzis, S. Lampaki, K. Zarogoulidis and P. Zarogoulidis. *Pleura space anatomy*. 2015. doi: 10.3978/j.issn.2072-1439.2015.01.48.
- Chiumello et al., 2016.** D Chiumello, D Consonni, S Coppola, S. Froio, Crimella F. and Colombo A. *The occlusion tests and end-expiratory esophageal pressure: measurements and comparison in controlled and assisted ventilation*. 2016. URL <https://pubmed.ncbi.nlm.nih.gov/26868503/>.

- Cushway et al., 2022.** J. Cushway, L. Murphy, J. Geoffrey, G. Shaw and T. Desai. *Modelling patient specific cardiopulmonary interactions*. 2022. doi: <https://doi.org/10.1016/j.compbimed.2022.106235>.
- Danchin et al., 1991.** A. Danchin, C. Medigue, O. Gascuel, H. Soldano and A. Hénaut. *From data banks to data bases*. 1991. doi: [10.1016/0923-2508\(91\)90073-j](https://doi.org/10.1016/0923-2508(91)90073-j).
- Dansk Intensiv Database, 2021.** Dansk Intensiv Database. *Dansk Intensiv Database Endelig version til offentliggørelse*, 2021. URL https://www.sundhed.dk/content/cms/12/4712_did_aarsrapport2021_offentligversion.pdf.
- Dellaca et al., 2017.** R. L. Dellaca, C. Veneroni and R. Farre. *Trend in mechanical ventilation: Are we ventilating our patients in the best possible way?* 2017. URL <https://www.ncbi.nlm.nih.gov/pmc/articles/PMC5467868/>.
- Duiverman et al.** M. L. Duiverman, S. A. Huberts, L. A. Eykern, G. Bladder and P. Wijkstra. *Respiratory muscle activity and patient–ventilator asynchrony during different settings of noninvasive ventilation in stable hypercapnic COPD: does high inspiratory pressure lead to respiratory muscle unloading?* doi: [10.2147/COPD.S119959](https://doi.org/10.2147/COPD.S119959).
- E. Brackett and Sanghavi.** D. E. Brackett and D. K. Sanghavi. *Pressure Support*. URL <https://www.ncbi.nlm.nih.gov/books/NBK482391/>.
- Feher, 2017.** J. Feher. *Quantitative Human Physiology*. 2017.
- Grieco L. and Chen L, 2017.** D. Grieco L. and Brochard L. Chen L. *Transpulmonary pressure: importance and limits*. 2017. URL <https://pubmed.ncbi.nlm.nih.gov/28828360/>.
- Hess R., 2014.** D. Hess R. *Respiratory mechanics in mechanically ventilated patients*. 2014. URL <https://rc.rcjournal.com/content/59/11/1773>.
- Matlab, 2023a.** Matlab. *ODE113*, 2023. URL <https://se.mathworks.com/help/matlab/ref/ode113.html>.
- Matlab, 2023b.** Matlab. *kstest*, 2023. URL <https://se.mathworks.com/help/stats/kstest.html>.
- Mauri et al., 2017.** T. Mauri, B. Cambiaghi, E. Spinelli, T. Langer and G. Grasselli. *Spontaneous breathing: a double-edged sword to handle with care*. 2017. doi: [doi:10.21037/atm.2017.06.55](https://doi.org/10.21037/atm.2017.06.55).
- Mineroff, 2019.** J. Mineroff. *Circopt*, 2019. URL <https://github.com/idealab-isu/CircoOpt>.

- Mineroff et al., 2019.** J Mineroff, AD McCulloch, D. Krummen, B. Ganapathysubramanian and A. Krishnamurthy. *Optimization Framework for Patient-Specific Cardiac Modeling*. 2019. doi: doi:10.1007/s13239-019-00428-z.
- Ochiai, 2015.** R. Ochiai. *Mechanical ventilation of acute respiratory distress syndrome*. 2015. URL <https://jintensivecare.biomedcentral.com/articles/10.1186/s40560-015-0091-6>.
- Pasteka et al., 2021.** R. Pasteka, Joao Santos C., N. Barros, R. Kolar and M. Forjan. *Patient-Ventilator Interaction Testing Using the Electro- mechanical Lung Simulator xPULM™ during V/A-C and PSV Ventilation Mode*. 2021. doi: 10.20944/preprints202103.0732.v1.
- Pham et al., 2017.** T. Pham, J. Brochard and A Slutsky. *Mechanical Ventilation: State of the Art*. 2017. doi: <https://doi.org/10.1016/j.mayocp.2017.05.004>.
- Pinsky, 2017.** R. M. Pinsky. *Cardiopulmonary Interactions: Physiological Basis and Clinical Applications*. 2017. doi: 10.1513/AnnalsATS.201704-339FR.
- Reese et al., 2018.** S. E. Reese, Dan K.S., Stieber K., S. Spadaro and T. Mauri. *An open-loop, physiological model based decision support system can reduce pressure support while acting to preserve respiratory muscle function*. 2018. URL <https://pubmed.ncbi.nlm.nih.gov/30317049/>.
- Roesthuis et al.** L. Roesthuis, J. Doorduyn, J. Van der Hoeven and L. M.A. Heunks. *Respiratory muscle recruitment during mechanical ventilation: Effects of ventilator settings*. doi: 10.1183/13993003.congress-2015.OA4955.
- Sieburg, 1990.** H. B. Sieburg. *Physiological Studies in Silico*. 1990. URL https://www.researchgate.net/profile/Hans-Sieburg/publication/309076709_Physiological_Studies_in_silico/links/5d276840458515c11c26a389/Physiological-Studies-in-silico.pdf.
- Team, 2024.** Circadapt Research Team. *CircAdapt*, 2024. URL <https://www.circadapt.org/>.
- Treboul et al., 2018.** J.L. Treboul, X. Monnet, D. Chemla and F. Michard. *Arterial Pulse Pressure Variation with Mechanical Ventilation*. 2018. doi: 10.1164/rccm.201801-0088CI.
- Van Osta et al., <https://doi.org/10.1098/rsta.2019.0347>.** Lyon A. Kirkels F. Van Osta, N. and, T. Koopsen, T. van Loon, M. J. Cramer, A. J. Teske, W. Delhaas T., Huberts and J. Lumens. *Parameter subset reduction for patient-specific modelling of arrhythmogenic cardiomyopathy-related mutation carriers in the CircAdapt model*. <https://doi.org/10.1098/rsta.2019.0347>. doi: <https://doi.org/10.1016/j.mayocp.2017.05.004>.

- Vicario et al., 2015.** F. Vicario, A. Albanese, D. Wang, N. Karamolegkos and N. Chbat. *Constrained Optimization for Noninvasive Estimation of Work of Breathing*. 2015. URL <https://pubmed.ncbi.nlm.nih.gov/26737494/>.
- Wallace and Regunath.** H. A. Wallace and H. Regunath. *Fluid Resuscitation*. URL <https://www.ncbi.nlm.nih.gov/books/NBK534791/>.
- Walmsley et al., 2015.** J. Walmsley, T. Arts, N. Derval, P. Bordachar, H. Cochet, S. Ploux, F. W. Prinzen, T. Delhaas and J. Lumens. *Fast Simulation of Mechanical Heterogeneity in the Electrically Asynchronous Heart Using the MultiPatch Module*. 2015. doi: doi:10.1371/journal.pcbi.1004284.
- Yoder, 2016.** B. A. Yoder. *Mechanical Ventilation: Disease-Specific Strategies*. 2016. URL <http://dx.doi.org/10.1016/B978-0-323-39006-4.00023-5>.
- Zhang et al., 2019.** B. Zhang, D. Ratano, L. Brochard, J. and T. Chan C. Y. *A physiology-based mathematical model for the selection of appropriate ventilator controls for lung and diaphragm protection*. 2019.
- Zielinska et al., 2018.** K. M. Zielinska, R. Krenke, M. E. Grabczak and R. W. Light. *PleuraL manometry-historical background, rationale for use and methods of measurement*. 2018. doi: <https://doi.org/10.1016/j.rmed.2018.01.013>.

A | Validation Test Protocol for UR03

Header:

Revision number	Rev 2
Protocol ID	VATP-UR03-V2
Author	Lasse Leuchtmann
Reviewer	Lasse Leuchtmann
Date created	5-11-2023
Date reviewed	19-12-2023

Protocol for testing UR03 - The solution must be able to simulate pressure support mechanical ventilation administered in the clinical trials

Prerequisites: Data from 3 patients from the clinical trials

1. Extract R_{aw} , C_{rs} , P_{mus} , T_{insp} , T_{exp} , PS, PEEP, TCT, T_{rise} , $P_{musinsp+deflate}$ as described in section 6.4.1
- 2 Simulate patient's breath with the respiratory module
- 3 Perform step 1-3 at every breath in the current timeframe in patient's clinical trial data
- 4 At each breath, perform CD comparison as described in section 6.4.3.1 on the following state variables: V_t , P_{aw} and $Flow$
- 5 Perform step 1-4 at every timeframe in the patients clinical trial data

Success if: CD at >50% of timeframes is >0.9

B | Validation Test Protocol for UR04

Header:

Revision number	Rev 2
Protocol ID	VATP-UR04-V2
Author	Lasse Leuchtmann
Reviewer	Lasse Leuchtmann
Date created	5-11-2023
Date reviewed	19-12-2023

Protocol for testing UR04 - The solution must be able to simulate cardiopulmonary interactions based on the clinical trial data

Prerequisites: Data from 3 patients from the clinical trials

1. Extract R_{aw} , C_{rs} , P_{mus} , T_{insp} , T_{exp} , PS, PEEP, TCT, T_{rise} , $P_{musinsp+deflate}$ as described in section 6.4.1
- 2 Extract PPV as described in section 6.4.1
- 3 Simulate the patient's respiratory breathing pattern using the respiratory module
- 4 Simulate the patient's cardiac cycle using the cardiovascular module
- 5 Simulate cardiopulmonary interactions by transducing P_{pl} from the respiratory module via the intrathoracic module, onto the P_{pa} from the cardiovascular module
2. Perform step 1-5 at every breath in the current timeframe
- 6 I the current timeframe perform CD comparison as described in section 6.4.3.1 on the following state variables: PPV
- 7 Perform step 1-7 at every timeframe in patient's clinical data

Success if: CD at >50% of timeframes is >0.9

C | Validation Test Protocol for UR05

Header:

Revision number	Rev 2
Protocol ID	VATP-UR05-V2
Author	Lasse Leuchtmann
Reviewer	Lasse Leuchtmann
Date created	5-11-2023
Date reviewed	19-12-2023

Protocol for testing UR05 - The solution must be able to simulate the surrogate P_{mus} derived from the clinical trials

Prerequisites: Data from 3 patients from the clinical trials

1. Extract R_{aw} , C_{rs} , P_{mus} , T_{insp} , T_{exp} , PS, PEEP, TCT, T_{rise} , $P_{musinsp+deflate}$ as described in section 6.4.1
- 2 Extract PPV as described in section 6.4.1
- 3 Simulate the patient's respiratory breathing pattern using the respiratory module
- 4 Perform step 1-4 at every breath in the current timeframe
- 4 In the current timeframe perform CD comparison as described in section 6.4.3.1 on the following state variables: P_{mus}
- 5 Perform step 1-5 at every timeframe in patient's clinical data

Success if: CD at >50% of timeframes is >0.9

D | Validation Test Protocol for SR01

Header:

Revision number	Rev 2
Protocol ID	VETP-SR01-V2
Author	Lasse Leuchtmann
Reviewer	Lasse Leuchtmann
Date created	7-11-2023
Date reviewed	25-12-2023

Protocol for testing SR01 - The system must be able to simulate the patient's respiratory physiology

1. Simulate the respiratory module with the following settings

Parameters	Value
Mechanical Properties	
C_{rs}	$25 - 70 \frac{mL}{cmH_2O}$ in increments of 2.5cmH2O
C_{cw}	$120 \frac{mL}{cmH_2O}$
Bulk Properties	
R_{aw}	$2-15 \frac{cmH_2O}{\frac{L}{s}}$ in increments of $1 \frac{cmH_2O}{\frac{L}{s}}$

Table D.1: Parameters at which to simulate the respiratory module

Inputs	Value
Vent Settings	
PS	2-30cmH2O in increments of 1cmH2O
PEEP	0-25cmH2O in increments of 1cmH2O
PSTrigger	0-(-2.5)cmH2O in increments of 0.25cmH2O
t_{insp}	0.75-2.5S in increments of 0.25S
t_{exp}	1-3.5S in increments of 0.25S
Rise Time	20% of t_{insp}
P_{mus} Settings	
Ti P_{mus}	Same as t_{insp}
Te P_{mus}	Same as t_{exp}
P_{mus} Set	0-25cmH2O in increments of 0.5cmH2O
P_{mus} Deflation time	0.2-1s in increments of 0.1S
Simulation Parameters	
Δt	0.02s
Simulation length	1TCT-10TCT at every simulation

Table D.2: Inputs at which to simulate the respiratory module

2. Simulate 50 scenarios with different combinations of the settings
3. At each simulation, validate the following state variables: P_{pl} , V_t , P_{aw} , $flow$
4. note any anomalies from expected values at each simulation (expected values vary depending on simulation, please discuss every potential anomaly with qualified personnel)

Success if: 45 out of 50 simulations fall within expected respiratory values.

E | Validation Test Protocol for SR02 + SR03 + SR04

Header:

Revision number	Rev 2
Protocol ID	VETP-SR01-V2
Author	Lasse Leuchtmann
Reviewer	Lasse Leuchtmann
Date created	7-11-2023
Date reviewed	25-12-2023

Protocol for testing the following requirements

- SR02 - The system must be able to simulate the intrathoracic pressure changes occurring as a result of respiration
- SR03 - The system must be able to simulate the cardiovascular system
- SR04 - The system must be able to simulate the cardiopulmonary interactions

1. Simulate the cardiovascular module with its default settings
2. Simulate the respiratory module with its default settings
3. Simulate the intrathoracic pressure module with the P_{pl} from the simulation performed in step 2
4. Plot P_{pl} and P_{aw} on top of P_{pa} for visual inspection
5. Numerically compare P_{pa} baseline with P_{pa} from step 2
- 5a Validate whether transfer of P_{pl} by a factor α corresponds to added P_{it} at P_{pa}

Success if: Success if step 5a validates correct transfer of P_{pl} by a factor α to added P_{it} at P_{pa}

F | Validation Test Protocol for SR05

Header:

Revision number	Rev 2
Protocol ID	VETP-SR05-V2
Author	Lasse Leuchtmann
Reviewer	Lasse Leuchtmann
Date created	7-11-2023
Date reviewed	27-12-2023

Protocol for testing SR05 - The system must be able to simulate spontaneous breathing

1. Simulate the respiratory module with the following settings

Parameters	Value
Mechanical Properties	
C_{rs}	$40 \frac{mL}{cmH_2O}$
C_{cw}	$120 \frac{mL}{cmH_2O}$
Bulk Properties	
R_{aw}	$2 \frac{cmH_2O}{\frac{L}{s}}$

Table F.1: Parameters at which to simulate the respiratory module

Inputs	Value
Vent Settings	
PS	2-12cmH ₂ O in increments of 1cmH ₂ O
PEEP	5cmH ₂ O
PSTrigger	-1.5cmH ₂ O
t_{insp}	1.5s
t_{exp}	2.5s
Rise Time	20% of t_{insp}
P_{mus} Settings	
Ti P_{mus}	Same as t_{insp}
Te P_{mus}	Same as t_{exp}
P_{mus} Set	0-25cmH ₂ O in increments of 0.5cmH ₂ O
P_{mus} Deflation time	0.2-1s in increments of 0.1S
Simulation Parameters	
Δt	0.02s
Simulation length	1TCT-10TCT at every simulation

Table F.2: Inputs at which to simulate the respiratory module

2. Simulate 50 scenarios with different combinations of the settings
3. At each simulation, validate the following state variables: P_{pl} , V_t , P_{aw} , $flow$
4. note any anomalies from expected values at each simulation (expected values vary depending on simulation, please discuss every potential anomaly with qualified personnel)

Success if: At least 45 out of 50 simulations correctly simulate spontaneous breathing

G | Validation Test Protocol for SR06

Header:

Revision number	Rev 2
Protocol ID	VETP-SR06-V2
Author	Lasse Leuchtmann
Reviewer	Lasse Leuchtmann
Date created	7-11-2023
Date reviewed	27-12-2023

Protocol for testing SR06 - The system must be able to simulate positive pressure ventilation

1. Simulate the respiratory module with the following settings

Parameters	Value
Mechanical Properties	
C_{rs}	$40 \frac{mL}{cmH_2O}$
C_{cw}	$120 \frac{mL}{cmH_2O}$
Bulk Properties	
R_{aw}	$4 \frac{cmH_2O}{\frac{L}{s}}$

Table G.1: Parameters at which to simulate the respiratory module

Inputs	Value
Vent Settings	
PS	12-35cmH ₂ O in increments of 1cmH ₂ O
PEEP	5-15cmH ₂ O in increments of 1cmH ₂ O
PSTrigger	-1.5cmH ₂ O
t_{insp}	1.5s
t_{exp}	2.5s
Rise Time	20% of t_{insp}
P_{mus} Settings	
Ti P_{mus}	Same as t_{insp}
Te P_{mus}	Same as t_{exp}
P_{mus} Set	0-25cmH ₂ O in increments of 0.5cmH ₂ O
P_{mus} Deflation time	0.6s
Simulation Parameters	
Δt	0.02s
Simulation length	1TCT-10TCT at every simulation

Table G.2: Inputs at which to simulate the respiratory module

2. Simulate 50 scenarios with different combinations of the settings
3. At each simulation, validate the following state variables: P_{pl} , V_t , P_{aw} , $flow$
4. note any anomalies from expected values at each simulation (expected values vary depending on simulation, please discuss every potential anomaly with qualified personnel)

Success if: At least 45 out of 50 simulations correctly simulate positive pressure ventilation

H | Respiratory Module

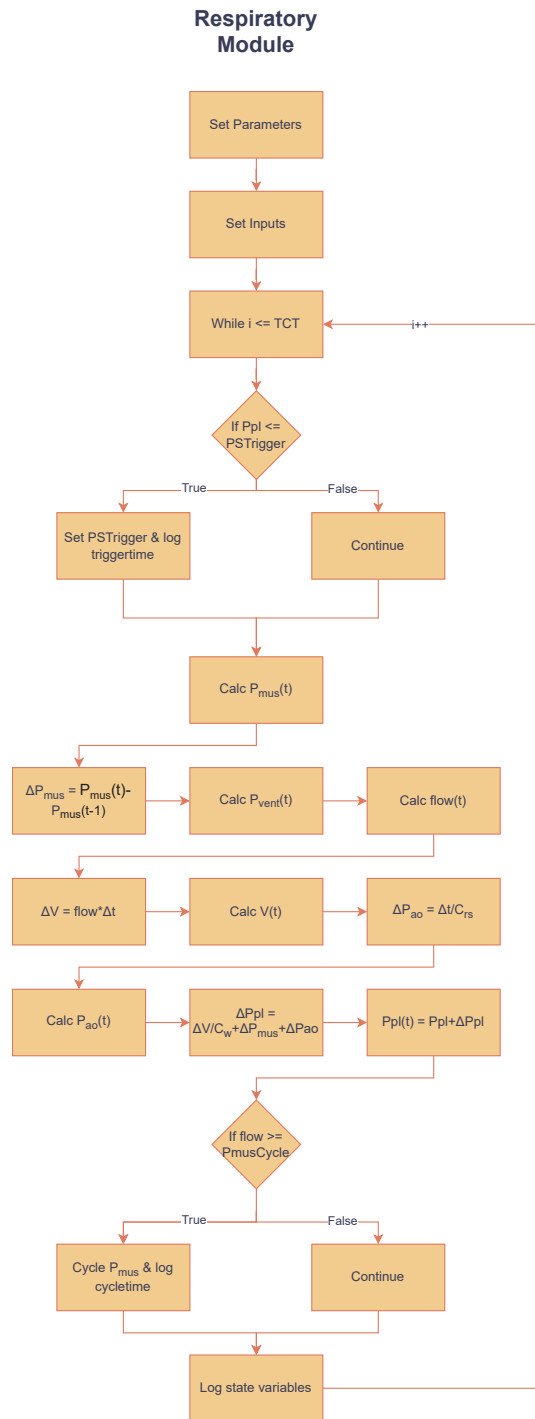


Figure H.0.1: The flowchart of the respiratory module of the cardiopulmonary interactions model. First, the parameters and then the inputs are set. For every Δt in the duration of TCT, the PSTrigger threshold is checked. Then, the time based driver functions described in section 6.1 provide P_{mus} and p_{vent} , after which the set of differential equations described in section 6.1 are calculated. Then, the flow threshold determining determination of respiratory cycle is checked, and state variables are logged.

I | Anatomy of Mechanical Ventilation

The basic functional units of a mechanical ventilator can be seen in figure I.0.1

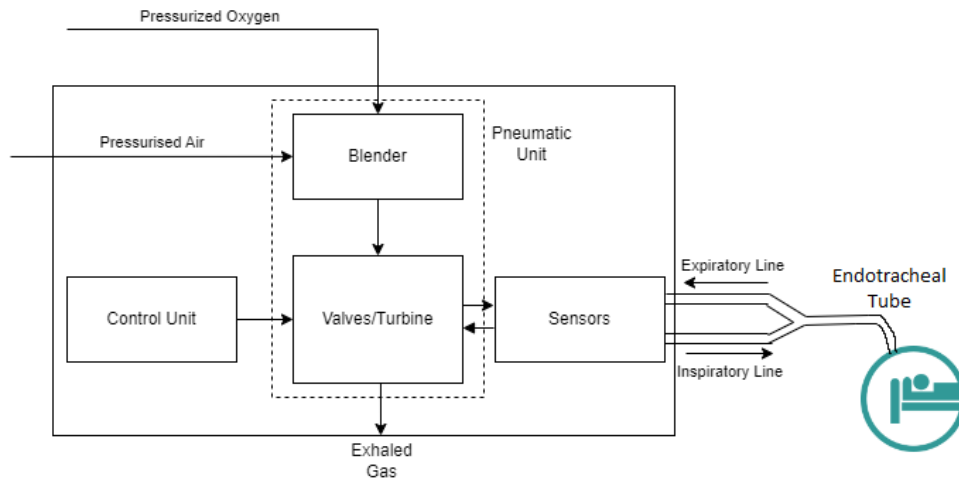


Figure I.0.1: The basic anatomy of a mechanical ventilator. Adapted from Pasteka et al. [2021]. Depicted are the blender, valve, sensors, control unit, expiratory line, inspiratory line, endotracheal tube as well as the gas flows throughout the system.

The basic functional units of a mechanical ventilator are [Dellaca et al., 2017]:

- **Pneumatic Unit:** *The pressure source used to overcome the elastic and resistive load of the patient's respiratory system*
- **Blender:** *The unit responsible for the air-O₂ ratio*
- **Valves:** *Several valves are necessary depending on the mechanical ventilator. They regulate the gas flow to- and from the patient*
- **Control unit:** *The control unit is responsible for adjusting the valves and turbines, in order to deliver the respiratory support to the patient*
- **Sensors:** *Sensors provide information regarding various physiological variables to the control unit*
- **Expiratory line:** *The line active during expiration*
- **Inspiratory line:** *The line active during inspiration*

- **Endotracheal tube:** *The endotracheal tube (ET) is put into the patients trachea. This allows the mechanical ventilator to support the patients respiratory system, by allowing air to flow in and out. An inflated balloon is placed on the ET, providing airway protection against unwanted substances, as well as providing an option for subglottic suctioning.*

J | Transmural pressures

Transmural pressures are referred to as the pressures inside relative to the outside of a compartment. Thus, transmural pressures denote whether a compartment expand or deflate. [Feher, 2017]

When considering the compartment model of the lungs depicted in figure J.0.1, there are three transmural pressures of interest. These are trans respiratory pressure (TRP), trans airway pressure (TAP) and trans thoracic pressure (TTP).

TRP is the pressure difference between P_{Paw} and P_{pl} , TTP is the pressure difference between P_{pl} and P_{Atm} , and lastly TRP is the pressure difference between P_{Paw} and P_{Atm} . [Feher, 2017]

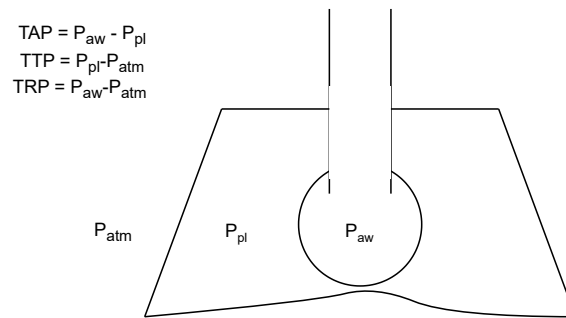


Figure J.0.1: A simplified model of the lung anatomy, adapted from Vicario et al. [2015]. Depicted are intracompartmental pressures of the airways (P_{aw}), pleural cavity (P_{pl}) and the atmosphere (P_{atm}). The transmural pressures are derived as $TAP = P_{aw} - P_{pl}$, $TTP = P_{pl} - P_{atm}$ and $TRP = P_{aw} - P_{atm}$.

K | Anatomy of the Pleural Cavity

The pleural cavity is a cavity encapsulated by the pleura, located between the lungs and chest wall. The pleura is a serous membrane, which functions to protect the lungs against friction with its attachment points during the respiratory cycle. [Charalampidis et al., 2015] The pleura is delineated into visceral- and parietal sections. The visceral pleura attaches directly to the lungs, and is thus inseparable from the lungs. The parietal pleura has several attachment points within the pleural cavity, as described in table K.1. [Charalampidis et al., 2015]

Anatomical Term	Attachment Points
Diaphragmatic Pleura	<i>Diaphragm</i>
Costal Pleura	<i>Thoracic cage (Ribs, intercostal muscles, costal cartilage)</i>
Cervical Pleura	<i>Neck</i>
Mediastinal Pleura	<i>Mediastinum</i>

Table K.1: Anatomical terms and attachment points of the different parts of the parietal pleura

The pleural cavity is bilaterally symmetrical. However, since the heart resides in the left side of the thoracic cavity, the left pleural cavity is smaller than the right. [Charalampidis et al., 2015] In the pleural cavity of an average adult male, resides 8-10mL of pleural fluid. The function of the fluid is to reduce mechanical stress caused by friction during the respiratory cycle. [Charalampidis et al., 2015]

L | Historical Perspective of Esophageal Manometry

The first registered use of esophageal manometry (EM) for P_{pl} measurements is dated to 1878, performed by Heinrich Irenaeus Quincke, in the context of pleural fluid withdrawal. Since then, EM saw widespread use in administering artificial pneumothorax for collapse therapy in the treatment of pulmonary tuberculosis. [Zielinska et al., 2018]

After the discovery of anti-tuberculous drugs, collapse therapy, and thus EM, was no longer performed. Zielinska et al. [2018]

During the 1980's and 1990's, EM was reintroduced into scientific studies. Since then, EM has been used for studying: [Zielinska et al., 2018]

- Thoracentesis
- Pleural fluid removal
- Unexpandable lung
- Delineation of trapped lung and lung entrapment

L.0.1 Complexity of Administering Esophageal Manometry

Two main methods of EM administration exist. These are water maonmeters and electronic systems. Their main advantages and disadvantages are described in table L.1

Advantages	Disadvantages
Water Manometer	
Low resource cost	Only mean P_{pl} measurements
Simple to administer	Sensible to movement artifacts from e.g. coughs.
Electronic Manometer	
Precise Measurements	More costly than water manometers
Possibility for local EM measurements, accounting for P_{pl} variations due to the pleura's anatomy	Validation of transducer placement is complicated
Simplifies digital data collection	

Table L.1: Major advantages and disadvantages of water based- and electronic manometers

M | CircAdapt

M.1 Cardiovascular Module

The base model for the system of equations governing the CVS is based on the CircAdapt model. CircAdapt is a full circulatory cardiovascular model, build as a hierarchy of components, simulating the physiology of various anatomical structures of the heart. Four types of structural components exist, as well as a global component governing the timing of the heart.

Fig M.1.1 shows examples of how each component relates to the CVS.

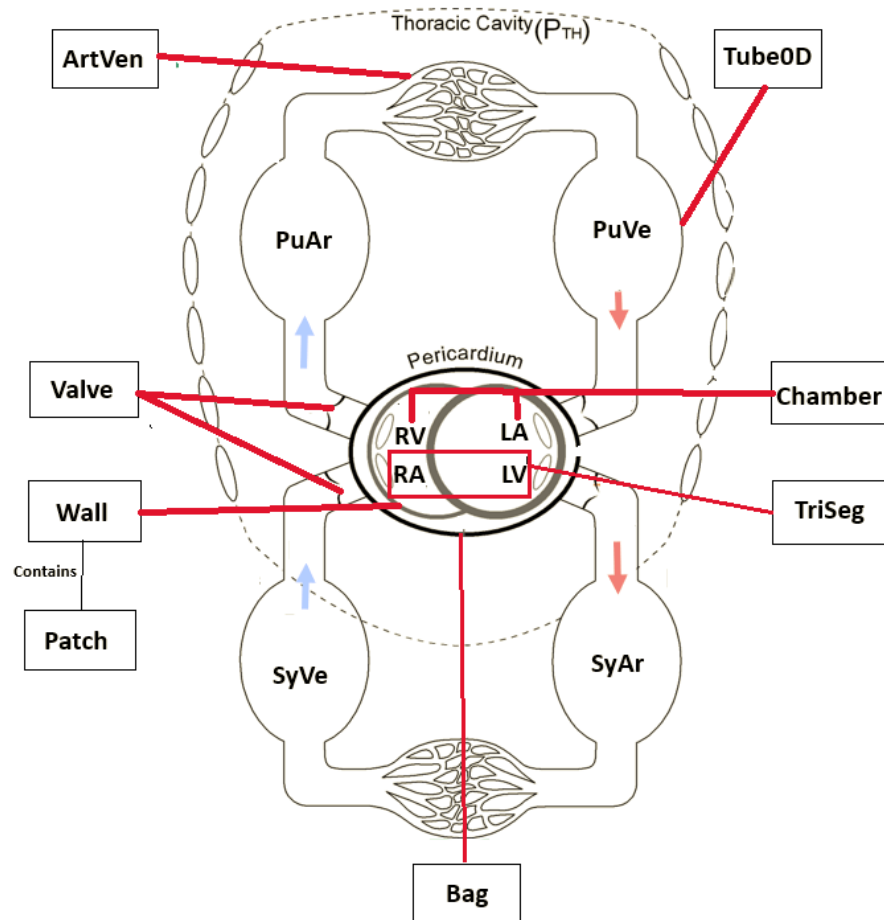


Figure M.1.1: examples of how the components of the CircAdapt framework relate to the CVS. ArtVen models the bloodflow between arteries and veins. Tube0D models the pressure/volume relationships of vessels. Valve models bloodflow between compartments of the CVS. Wall contains the Patch module, and combined they model surface area and myocardial contraction of each compartment. Chamber models the atria. TriSeg models the ventricles, and lastly Bag models the pericardium.

The four component types will be presented individually.

M.1.1 Node Component Hierarchy

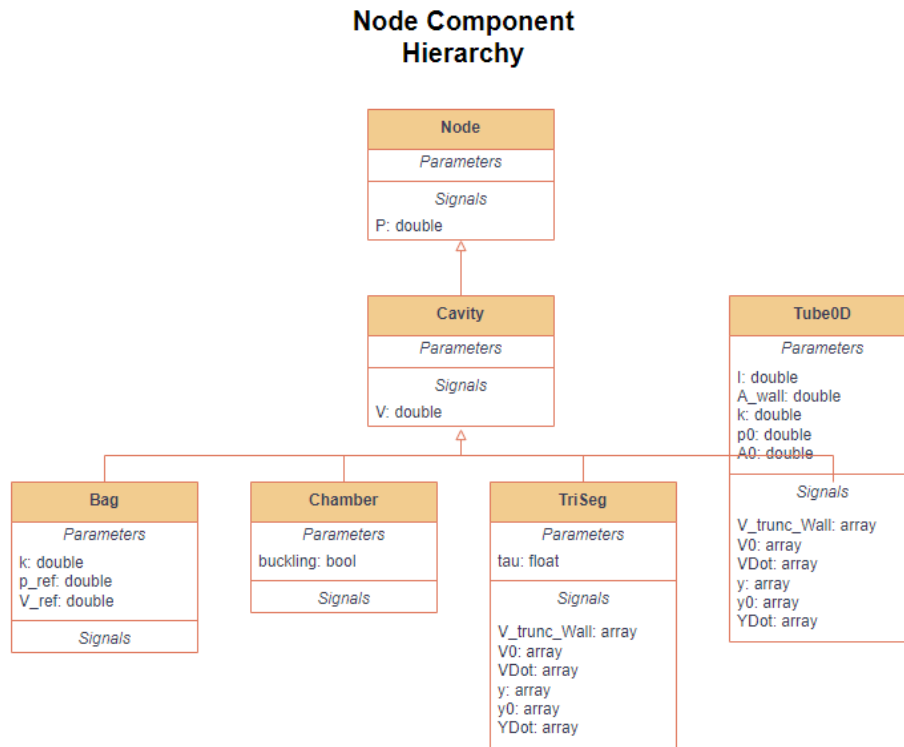


Figure M.1.2: Caption

Node

Node is the parent object of all node-type components, is an object with pressure as a state variable.

Cavity

A cavity component is a child object of the node component, with the volume state variable, related to the pressure inside the cavity.

Four child objects are derived from the cavity component.

Bag

The Bag component simulates the pericardium. It encapsulates all other components which constitute the heart. Thus, it adds a transmural pressure to the heart, related to the time-dependent volume of the components of the heart.

Eq 11 shows how the governing equation of transmural pressure within the Bag component:

$$p_{transmural}(V) = p_{ref} * \frac{V^k}{V_{ref}} \text{ (eq 11)}$$

Chamber

The chamber component simulates atria of the heart. It has a volume and a pressure, as well as wall and patch components governing the behavior of the chamber.

Chamber has two governing equations. The first calculates wall tension, the second calculates pressure.

The equation governing wall tension is described in eq 12:

$$T = \frac{\Delta t}{\Delta A_m} - (A_m - A_{m,0}) \text{ (eq 12)}$$

Where T is wall tension, A_m is wall area, and $A_{m,0}$ is the zero-tension midwall area.

The equation governing pressure inside the chamber is described by eq 13:

$$p_c = \frac{T * \Delta A_m}{\Delta V_m}$$

Where V_m is the mid-wall volume.

TriSeg

The TriSeg component models the left and right ventricles of the heart, as a connected segment separated by a wall.

The volume encapsulated by the walls of the right- and left ventricles is defined by the governing equations described in eq 14 and eq 15:

$$V_{Left} = V_{cLeft} + 0.5 * V_{wLeft} + 0.5V_{wSeptal} \text{ (eq 14)}$$

$$V_{Right} = V_{cRight} + 0.5 * V_{wRight} + 0.5V_{wSeptal} \text{ (eq 15)}$$

Where V_c is the volume of the cavity, V_w is the volume of the midwall, and $V_{w\text{Septal}}$ is the volume of the septal wall.

Tube0D

The Tube0D component models the pressures and volumes inside the vessels of the CVS.

The governing equations for area of the tube is described in eq 16:

$$A = \frac{V}{Len}$$

Where A is the area, V is the volume and Len is the length of the vessel

Eq 17 describes the governing equation

M.1.2 Patch Component Hierarchy

Patch Component Hierarchy

Patch
<i>Parameters</i>
Am_ref: double
V_wall: double
v_max: double
l_se: double
l_s0: double
dl_s_pas: double
Sf_pas: double
k1: double
tr: double
td: double
time_act: double
Sf_act: double
dt: double
C_rest: double
l_si0: double
LDAD: double
ADO: double
LDCC: double
Sf_pasMaxT: double
Sf_pasActT: double
FacSf_actT: double
LsPasActT: double
adapt_gamma: bool
<i>Signals</i>
l_s: array
l_si: array
LsiDot: array
C: array
C_dot: array
Am: array
Am0: array
Ef: array
T: array
dA_dT: array
Sf: array
Sf_pasT: array
SfEcm: array
dSf_dEf: array
dSf_pas_dEf: array
SfEcmMax: array
Sf_actMax: array
Sf_pasAct: array
LsPasAct: array

The patch component models the contraction of the myocardial muscle tissue. It assumes that all sar-

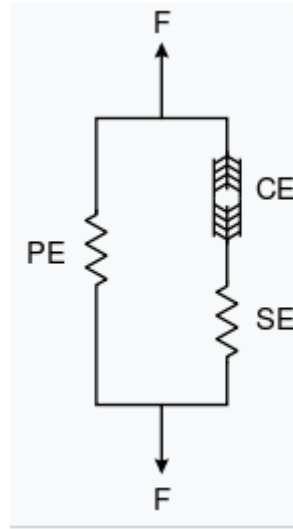


Figure M.1.3: Caption

comeres are identical in size and force generation.

Each sarcomere is modelled as a three-element Hill contraction model, depicted in fig 5.

Fig 5 The Hill Contraction Model. Sarcomeres are modelled as a contractile element (CE), which pull on a series elastic element (SE). Examples of SE are tendons, apnoeurosis or the proteins of the extracellular matrix (ECM). In parallel with the SE, a parallel elastic element (PE) is passively pulled upon. Examples of PE's are cell membrane and connective tissues.

Eq 17 governs the rate of change of the length of the sarcomeres:

$$\frac{\Delta l_{si}}{\Delta t} = v_{\max} * \left(\frac{l_s - l_{si}}{l_{se}} - 1 \right) \quad (eq\ 17)$$

Where v_{\max} is the sarcomere shortening rate, l_s the initial sarcomere length, l_{si} the current sarcomere length and l_{se} the length of the SE.

The contractility curve, representing the density of cross-bridges in the sarcomere, is governed by eq 18:

$$\frac{\Delta C}{\Delta t} = \frac{C_L(l_{si})}{\tau_{rise}} * F_{rise}(t) - \frac{C}{\tau_{decay}} * g(X) \quad (eq\ 18)$$

Where $\tau = 0.33 * T_d * t_{duration}$, $F_{rise}(t)$ is the activation function, $C_L(l_{si})$ the crossbridge formation

function and $g(X)$ the decay function.

Eq 18 has two function components. One describes the amount of cross bridges at a given time, the second component describes the decay of cross bridges at the given time. The ΔC is thus defined, by the change in cross-bridge formations vs. cross-bridge decays.

M.1.3 Connector component hierarchy

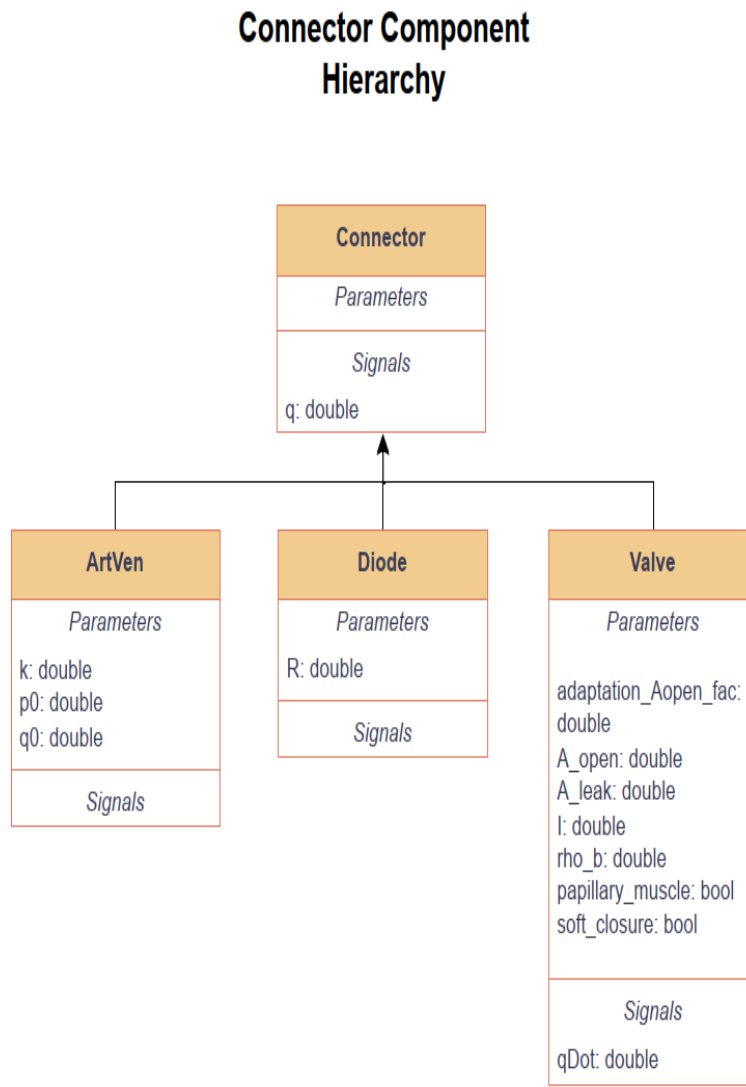


Figure M.1.4: Caption

Connectors are components allowing bloodflow between nodes. CircAdapt actively uses two types of connectors, the ArtVen and Valve components.

ArtVen

ArtVen, short for arteriovenous, models the bloodflow at the pulmonary- and systemic capillaries between the arteries and veins.

The bloodflow is governed by eq 20:

$$q = \Delta p * q_0 \left(\frac{|\Delta p|}{p_0} \right)^k \quad (eq\ 20)$$

Where q is flow, Δp is change in pressure, q_0 is initial flow and k is an exponent constant

Valve

The valve component models flow between nodes. In the full CVS model, the valve component is responsible for simulating the flow between the atrioventricular valves (mitralvalve and tricuspid valve), as well as the ventriculoarterial valves (aortic valve and pulmonary valve).

Flow through the valve is governed by the unsteady Bernoulli equation, described in eq 21

$$\frac{\Delta q}{\Delta t} = \frac{A_{valve}}{l_{valve}} \left(\frac{\Delta p}{\rho} - \frac{1q * |q|}{2} * \left(\frac{1}{A_{valve}^2} - \frac{1}{A_p^2} \right) \right)$$

With ρ being blood density, l_{valve} being length of the valve, A_{valve} is cross sectional area of the valve, A_p is cross sectional area proximal to valve.

For the unsteady Bernoulli equation to be applicable, the valve component assumes that:

- Gravity can be ignored
- Inertia is estimated through $E_{kin} = 0.5Lq^2$
- Velocity is estimated through flow divided by area
- Flow entering the valve has all pressure-flow energy converted to kinetic energy
- Flow out of the valve does not regain pressure, due to loss of energy from turbulence

M.1.4**M.1.5 Wall Component Hierarchy****Wall Component
Hierarchy**

Wall
<i>Parameters</i> Am_dead: double n_patch: int
<i>Signals</i> Am: array Am0: array Cm: array dA_dT: array p_trans: array T: array Vm: array V_wall: double

Figure M.1.5: Caption

N | Model Performance on Individual Timechunks

In order to diagnose the results of the full patient trial The following section presents results from patient data which has been processed through the framework described in section 5.1

Fig N.0.1

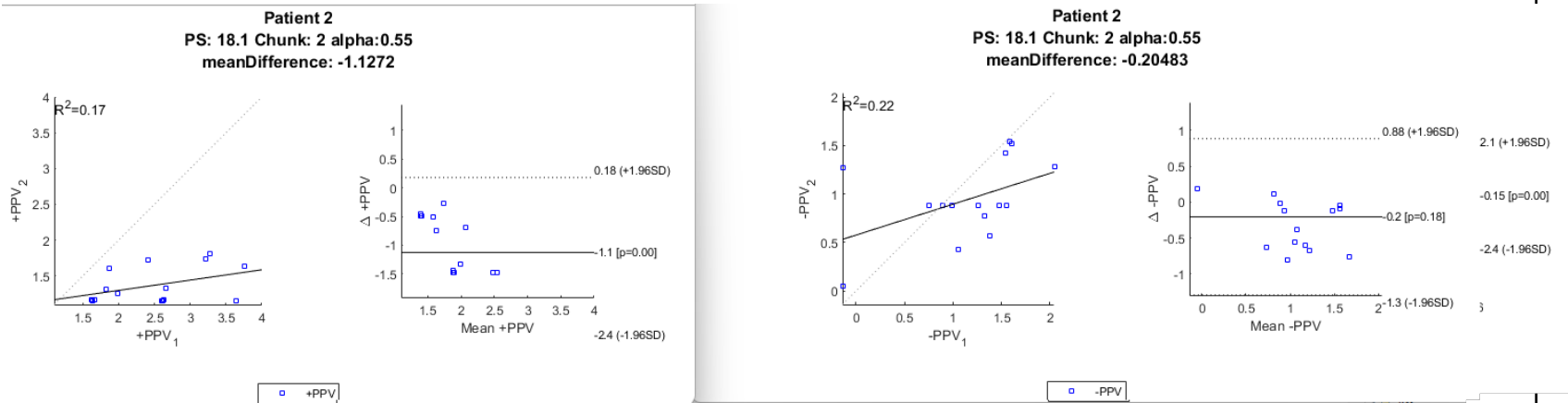


Figure N.0.1: Caption

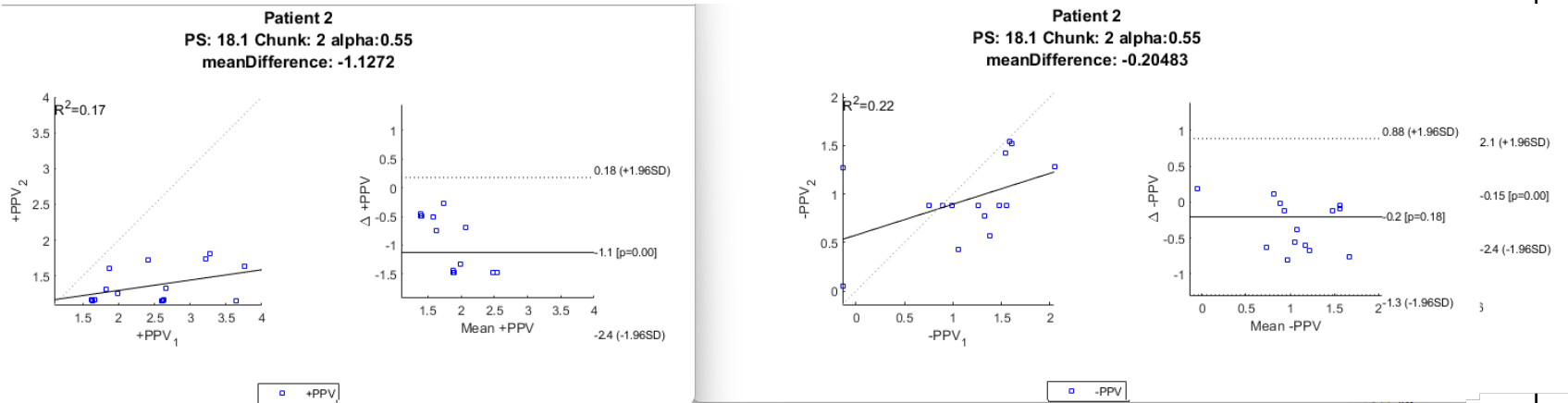


Figure N.0.2: Caption

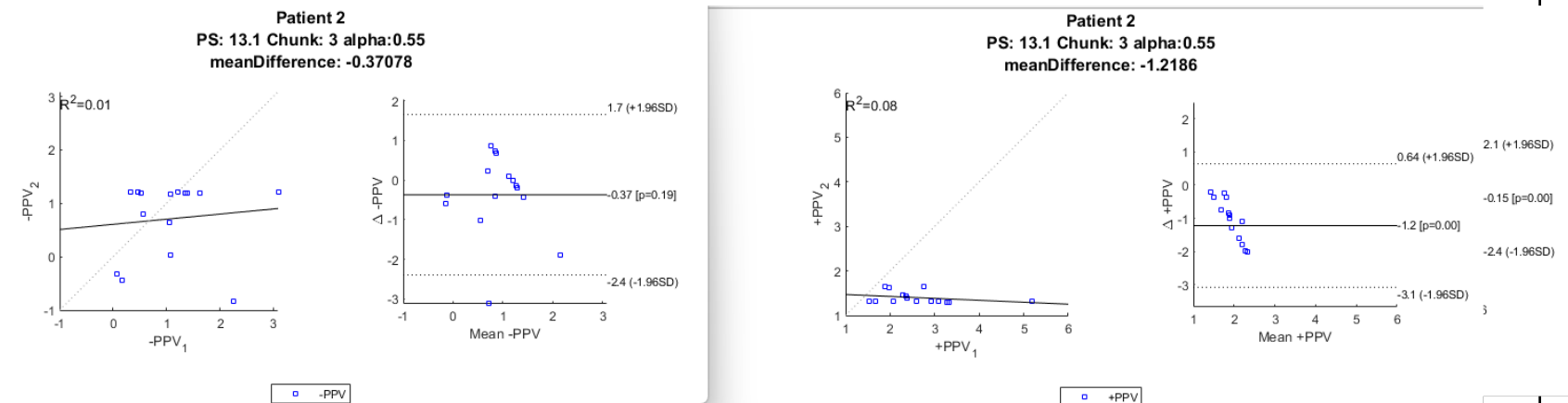


Figure N.0.3: Caption

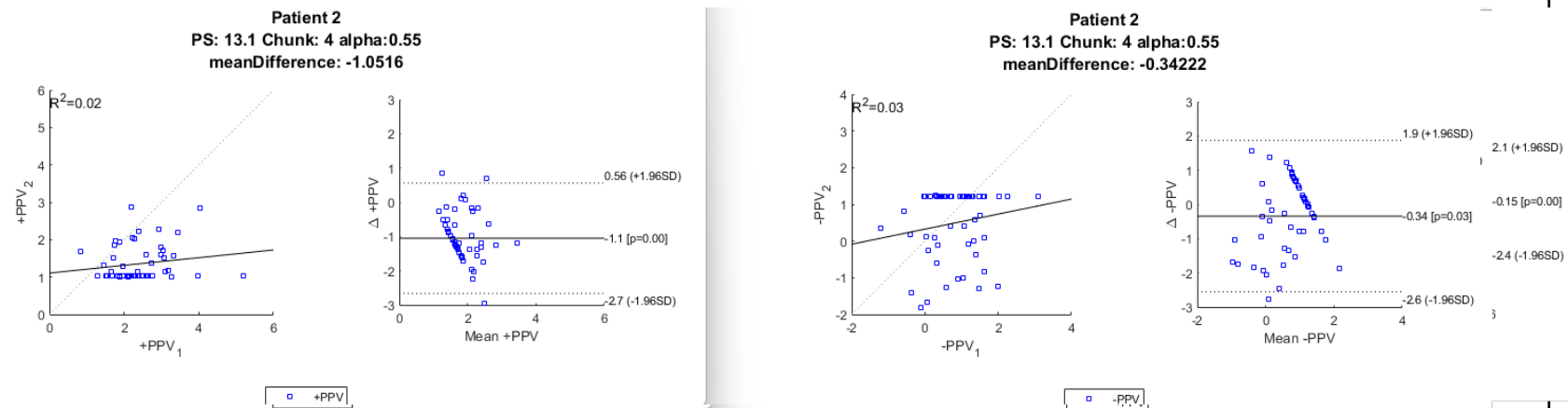


Figure N.0.4: Caption

N.0.1 Blood Pressure Predictions

In order to diagnose improvement potential of the model, its ability to diagnose P_a was tested.

Examples of the models performance on predicting +PPV/-PPV are highlighted in figure N.0.5, ??, figure N.0.7, figure N.0.8, figure N.0.9, figure N.0.10, figure N.0.11 and figure N.0.12.

Each timeframe within the clinical trial, had the patient on different PS levels, in order to test the hypothesis described in section 2.7. Each timeframe consists of a set of chunks where heartbeat to respiratory frequency is $>3.4 \frac{beats}{breath}$.

Refer to ?? for the performance on the remaining timeframes of the clinical trial.

N.0.2 Timeframe 1 - PS 18.1

Fig figure N.0.5 shows the results of the +PPV simulations in the 1st chunk of the PS 18.1 timeframe.

The simulations resulted in $R^2 = 0.48$, and a mean difference between simulated and observed measurements of -0.87292mmHg.

This indicates that 48% of the variability within the +PPV measurements can be explained by the regression model. Furthermore, the residual plots show a tendency for the residuals to be close to the regression line, indicating predictions close to measurements. The residual differences are show a tendency to evenly over- and underestimate +PPV.

The Bland-Altman plot indicates a cluster of differences close to and slightly below 0. Similarly to the residual plot, this indicates that this cluster has predictions close to measurements. The Bland-Altman plot also shows a tendency for underestimating +PPV. All measurements are within the limits of agreement (LOA), with most measurements falling within 1 standard deviation (STD) from the mean. One outlier is close to the negative LOA, but does not cross it.

A mean difference of -0.872mmHg confirms, that most predictions are close to measurements, with a slight tendency for underestimating +PPV.

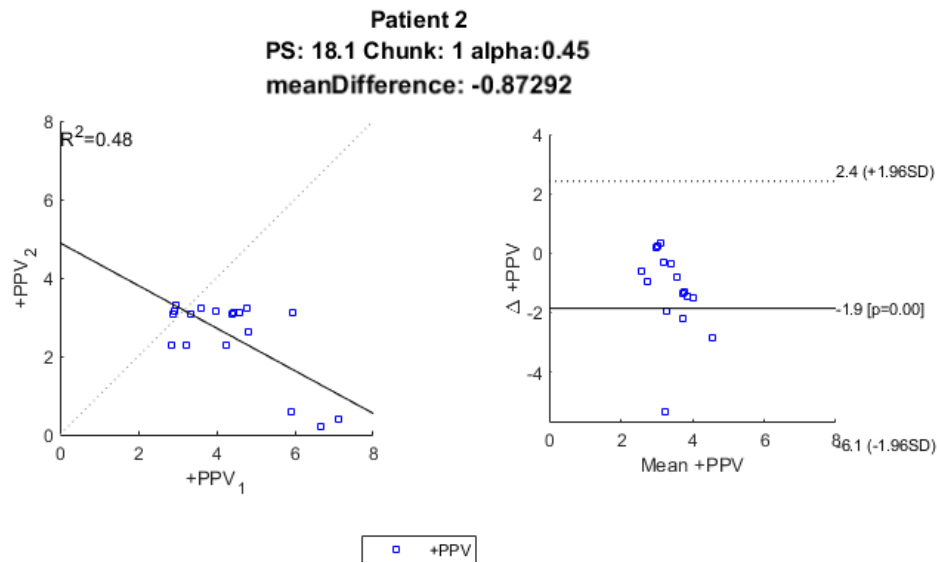


Figure N.0.5: +PPV for the 1st chunk of the PS 18.1 timeframe. $R = 0.48$ indicates that 48% of the variability within the measurements are explained by the regression model. The residual plot shows an even clustering around the regression line, with a slight tendency for underestimation. The Bland-Altman plot shows a clustering around the zero-difference line, with a tendency for slight underestimation. All measurements fall within the LOA, with most measurements being within +1STD, a few within -1STD and one outlier closer to -1.96STD. A mean difference of -0.872mmHg confirms the trend for slight underestimation of +PPV.

Figure N.0.5 shows the results of the -PPV predictions in the 1st chunk of the PS 18.1 timeframe.

The simulations resulted in $R^2 = 0.21$, and a mean difference between predicted and observed measurements of -0.01mmHg.

In figure N.0.5, 21% of the -PPV measurements can be explained by the regression model. The residual plots indicate a trend to evenly over- and underestimate -PPV. However, as opposed to +PPV, -PPV residuals are of a larger magnitude.

The Bland-Altman plot shows a scattering around the zero difference line. The observations are evenly under- and overestimated, confirming the trend of the residual plots. Most observations fall within 1STD, with 1 outlier falling below the negative LOA. This indicates normally distributed data, and measurement errors within the acceptable ranges.

A mean difference of -0.0112mmHg, shows that the average of the predictions slightly underestimates the measurements.

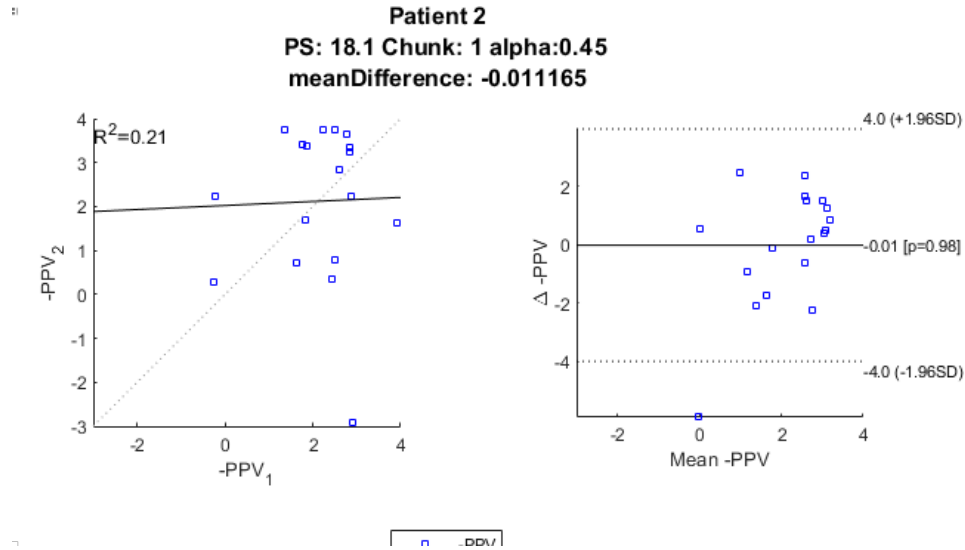


Figure N.0.6: -PPV for 1st chunk of PS 18.1 timeframe. An $R^2 = 0.21$ indicates that 21% of the variability in the model is explained by the regression line. The residual plots show an even tendency for over- and underestimating -PPV. The Bland-Altman plot shows scattering around the zero-difference line, with an even tendency to over- and underestimate -PPV, confirming the interpretation of the residual plot.

Fig N.0.7 shows the prediction of +PPV within the 2nd chunk of the PS 18.1 timeframe.

The predictions yielded an $R^2 = 0.34$, indicating that the regression line explains 34% of the variability within the model.

The residual plot shows a dense distribution around the regression line, with only 1 outlier prediction, indicating that most predictions fall close to the +PPV measurements.

The Bland-Altman plot shows that most observations are closely scattered around 4mmHg mean +PPV. With the exception of 1 outlier, all measurements fall within the LOA. The majority of observations fall within +1STD, with a few approaching +1.5STD. A few observations fall within -1STD, and 1 outlier is below -1.96STD. These observations confirm the normal distribution of the data.

A mean difference of -0.123mmHg indicates a slight tendency for underestimation. However, if the outlier measurement was discarded, a slight tendency for overestimation would be observed.

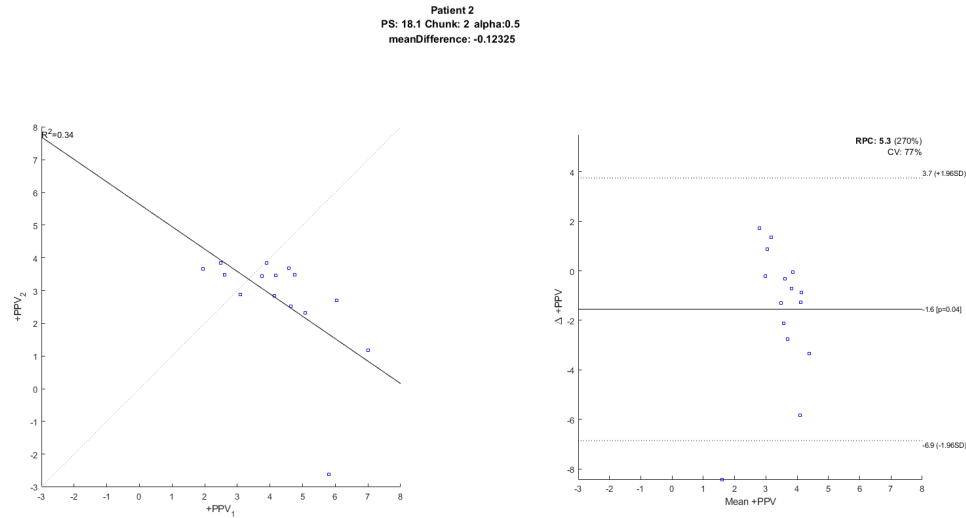


Figure N.0.7: $+PPV$ for the 2nd chunk of the PS 18.1 timeframe. An $R^2 = 0.34$ indicates that 34% of the variability within the model is explained by the regression line. The residual plots show a dense distribution around the regression line, indicating that predictions are close to measurements. The Bland-Altman plot shows that most observations fall closely within 4mmHg mean $+PPV$. Except for a single outlier, all observations fall within the LOA. -0.123mmHg mean difference indicates a tendency for the model to underestimate, however overestimation is judged to be the case if the outlier was discarded.

Fig figure N.0.8 shows the results of the $-PPV$ predictions in the 2st chunk of the PS 18.1 timeframe.

The model's predictions resulted in $R^2 = 0.21$, and a mean difference between observations of 0.149mmHg .

The R^2 indicates that 21% of the predictions can be explained by the regression model. The residual plots are horizontally distributed around the regression line, with close to even distribution of under- and over-estimation, with a slight tendency for overestimation. The horizontal distribution indicates that the regression model does not explain the observations accurately.

The Bland-Altman plot shows a tendency for the data to be horizontally scattered between $2.5\text{--}4\text{mmHg}$ mean $-PPV$. 33% of the observations are close to the zero-difference line, with 80% of the observations falling within $+1\text{STD}$ and -1STD . Two measurements fall right below the positive- and negative LOA respectively.

A mean difference of 0.149mmHg indicates a trend for the predictions to average the measurements, with a slight tendency for overestimation.

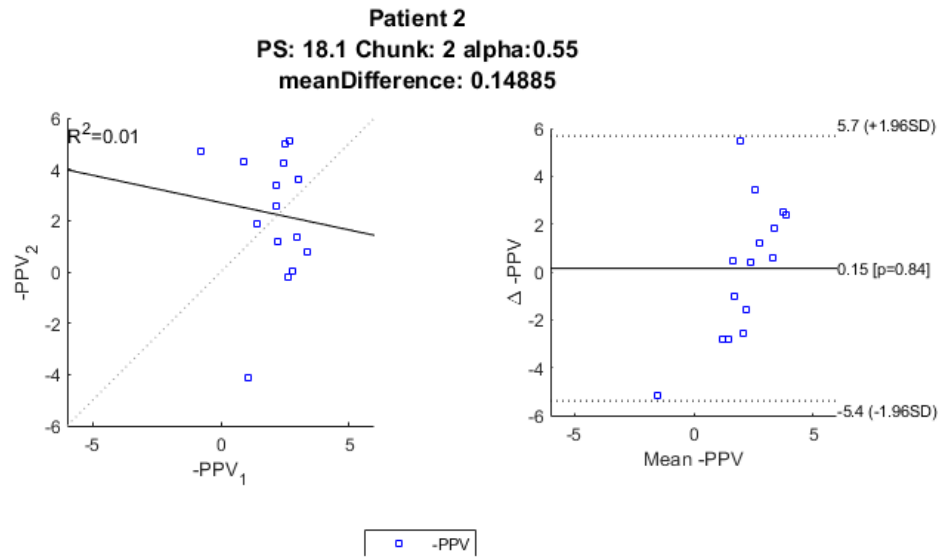


Figure N.0.8: -PPV for the 2nd chunk of the PS 18.1 timeframe. An $R^2 = 0.01$, combined with the pattern of horizontal distribution of the data, indicates that the regression model does not explain the observations accurately. The Bland-Altman plot shows a cluster of horizontal distributions of observations between 2.5-4mmHg. The observations follows a normal distribution, with two outliers tangential the positive- and negative LOA.

N.0.3 Timeframe 2 - PS 13.1

Fig N.0.9 shows the prediction of +PPV within the 1st chunk of the PS 13.1 timeframe.

The predictions yielded $R^2 = 0.01$, indicating that the regression model does not explain the observations properly.

The Bland-Altman plot shows that 64% of observations fall within +1STD. 28% of observations fall within -1STD, and 1 outlier falls below the negative LOA. This confirms the normal distribution of the observations.

A mean difference of -0.112mmHg +PPV indicates a slight tendency for the model to underestimate on average, however the tendency would presumably be overestimation if the outlier was discarded. The Bland-Altman plot supports this interpretation, as most observations fall within ± 2 mmHg.

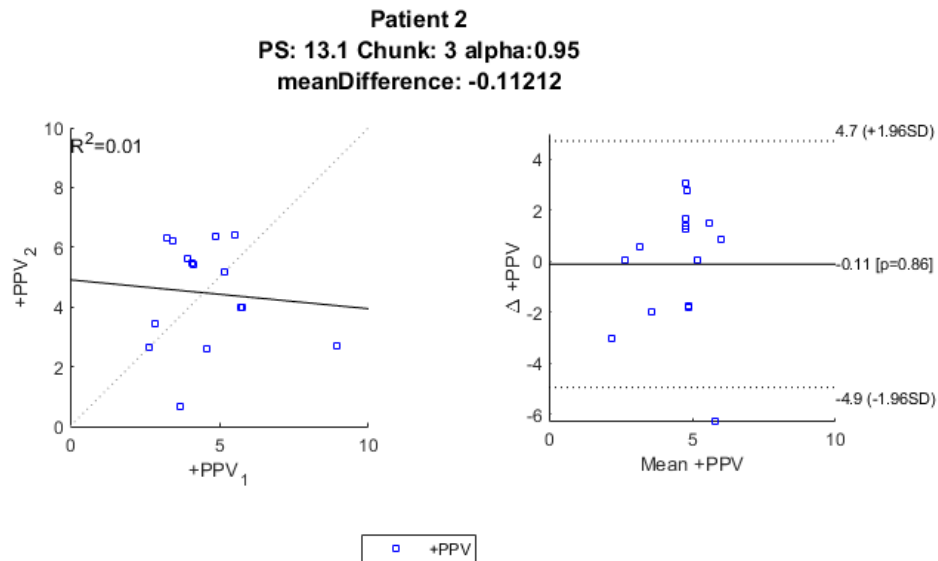


Figure N.0.9: +PPV for the 1st chunk of the PS 13.1 timeframe. Note, that this is the 3rd chunk in the total trial length. The regression model was unable to explain the variance of the observations. However, the Bland-Altman plot shows a clear normal distribution pattern, with 71% of observations falling within ± 2 mmHg. This indicates a pattern for the predictions to be close to the measurements on average.

Fig N.0.10 shows the -PPV predictions for the 1st chunk in the 13.1 PS timeframe of the clinical trial.

With a $R^2 = 0.01$, and an almost U-shaped distribution of the observations, the regression model is unable to provide valuable insight in the analysis. However, the residual plot shows a tendency for slight under- and overestimation, with the pattern favoring overestimation.

The Bland-Altman plot shows that 50% of the observations fall within -1STD, and 40% of observations fall within or slightly above +1STD. One outlier lies below the negative LOA. This indicates a normal distribution pattern.

With a mean difference of -0.873mmHg -PPV, the model shows that the model on average predicts the -PPV accurately, with a slight tendency for underestimation. If it is assumed, that the mean difference would be closer to 0, if the outlier measurement was discarded.

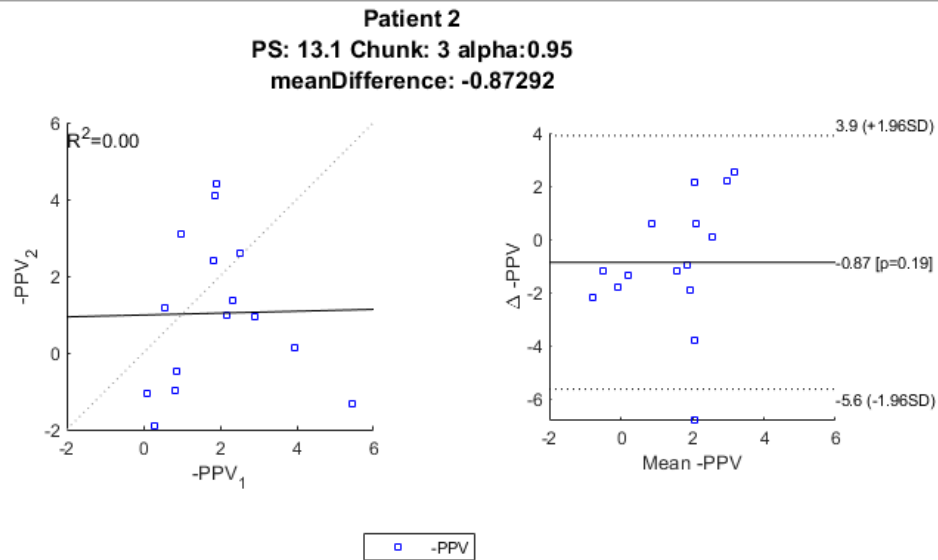


Figure N.0.10: -PPV for the 1st chunk of the PS 13.1 timeframe. Note, that this is the 3rd chunk of the total trial length. The regression model was unable to reliably explain the observations. The residual plots show a tendency for near-evenly distributed over- and underestimations. The Bland-Altman plots confirms a normal distribution of the observations. With a mean difference of -0.873mmHg, and the even distribution around mean, the measurement differences are assumed to be close to 0 on average.

Fig N.0.11 shows the results of +PPV simulation on the 2nd chunk of the PS 13.1 timeframe. Note, that this timeframe is significantly longer than the others included in the results section, and thus contains 55 observations.

Since the observations are tightly clustered around 5mmHg on the x-axis, the regression model does not provide valuable insight. However, the distribution plot indicates an even distribution of observed residuals, falling within -2mmHg and 4mmHg, indicating that most residuals systematically fall within this range.

The Bland-Altman plot shows that 60% of observations fall within ± 1 STD, with 20% landing within ± 1.70 STD. Of the remaining 20%, 13% are within positive and negative LOA, and 7% below the negative LOA. This indicated a normal distribution of the observations.

With a mean difference of -1.45mmHg +PPV, the normal distribution as well as the visually observed clustering around the mean, indicates that the models predictions are close to measurements on average.

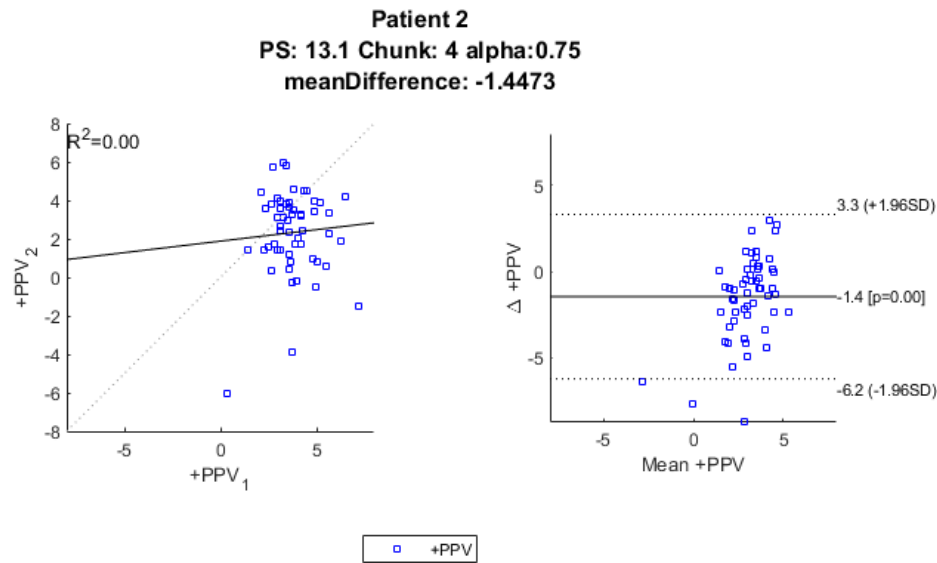


Figure N.0.11: +PPV for the 2nd chunk of the PS 13.1 timeframe. Note, that this is the 4th chunk in the total trial length. The regression model does not provide valuable insight. The Bland-Altman plot shows a normal distribution pattern. With a mean difference of -1.45mmHg +PPV, the models predictions are assumed to be close on average.

Fig N.0.12 shows the results of the -PPV simulation on the 2nd chunk of the PS 13.1 timeframe.

With an $R^2 = 0.30$, the regression model is able to explain 30% of the variance in the observations. The residual plot shows a dense vertical distribution around the regression line, with a cluster between 0 to 5mmHg. The distribution indicates a trend for the predictions slightly over- and underestimate the measurements.

The Bland-Altman plot shows 65% of the observations landing between ± 1 STD, 85% between 1.7STD and 95% within the LOA. 2 observations, constituting 4% of the data, fall beyond the negative and positive LOA, respectively. These observations indicate a normal distribution of the data.

With 55 observations, and a mean difference of -1.1451mmHg -PPV, the model is assumed to correctly predict -PPV on average. However, with 20% of the observations having a mean difference between -4mmHg and -6mmHg, the model has a tendency for largely underestimating the measurements.

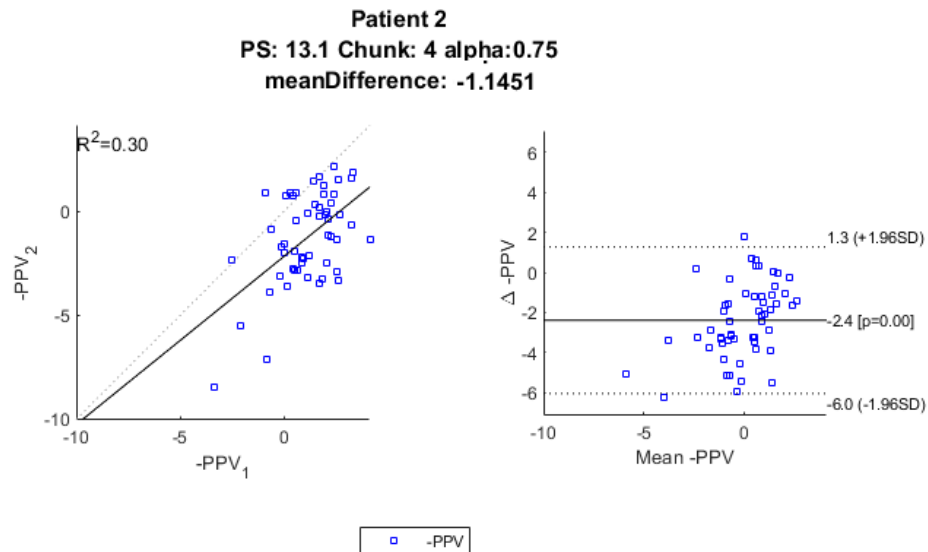


Figure N.0.12: -PPV for the 1st chunk of the PS 13.1 timeframe. Notw, that this is the 4t chunk of the total trial length. An $R = 0.30$ indicates a good fit of the regression to the observed residuals. The Bland-Altman plot shows a clear normal distribution. With a mean difference of -1.1451mmHg -PPV , it is assumed that the model correctly predicts -PPV on average. However, the model has a trend of largely underestimating individual measurements.

Table N.1 shows the results for every part of the clinical trial. The results will be further elaborated in the discussion.

N.0.4 Performance on entirety of patient data

The results of the individual chunk diagnosis indicated that the model had significantly lower accuracy at $PS = 3.1$ and $PS = 2.1$. Thus, the performance of the model of the entirety of the patient data was tested with and without these chunks.

Chunk	PS	Mean Diff [+PPV , -PPV] H_2O	R^2 [+PPV , -PPV]
1	18.1cm H_2O	[0.48 , 0.21]	[-0.87 , -0.01]
2	18.1cm H_2O	[0.34 , 0.21]	[-0.123 , 0.15]
3	13.1cm H_2O	[0.01 , 0.01]	[-0.11 , -0.873]
4	13.1cm H_2O	[0.00 , 0.3]	[-1.45 , -1.15]
5	13.1cm H_2O	[0.03 , 0.05]	[-0.03 , -1.20]
6	13.1cm H_2O	[0.14 , 0.37]	[-0.03 , -1.20]
7	13.1cm H_2O	[0.17 , 0.08]	[-0.08 , -0.0007]
8	13.1cm H_2O	[0.0.03 , 0.01]	[0.35 , -0.07]
9	10.1cm H_2O	[0.01 , 0.01]	[-1.22 , -0.62]
10	10.1cm H_2O	[0.09 , 0.04]	[-0.23 , -0.15]
11	10.1cm H_2O	[0.53 , 0.90]	[-0.02 , 0.2]
12	10.1cm H_2O	[0.20 , 0.90]	[0.09 , 1.30]
13	8.1cm H_2O	[0.33 , 0.75]	[-0.058 , 0.42]
14	8.1cm H_2O	[0.04 , 0.03]	[1.64 , 3.9]
15	6.1cm H_2O	[0.14 , 0.37]	[-0.03 , -1.20]
16	6.1cm H_2O	[0 , 0.89]	[0.188 , 2.27]
17	3.1cm H_2O	[0.02 , 0.92]	[1.47 , 3.15]
18	3.1cm H_2O	[0.62 , 0.0]	[3.87 , 5.97]
19	2.1cm H_2O	[0.20 , 0.027]	[3.26 , 6.1]
20	2.1cm H_2O	[0.78 , 0.33]	[2.5 , 5.59]

Table N.1: Table of results for the remaining timechunks. Refer to chapter 8 for the analysis of these results.